Non-linear release dynamics for a CeO2 nanomaterial embedded in a protective wood stain, due to matrix photo-degradation

Lorette Scifo, Perrine Chaurand, Nathan Bossa, Astrid Avellan, Melanie Auffan, Armand Masion, Bernard Angeletti, Isabelle Kieffer, Jérôme Labille, Jean-Yves Bottero, et al.

Non-linear release dynamics for a CeO_2 nanomaterial embedded in a protective wood stain, due to matrix photo-degradation

Lorette Scifo [a,b], Perrine Chaurand [b], Nathan Bossa [b], Astrid Avellan [b], Mélanie Auffan [b], Armand Masion [b], Bernard Angeletti [b], Isabelle Kieffer [d], Jérôme Labille [b], Jean-Yves Bottero [b] and Jérôme Rose [b].

AFFILIATION.

[a] *Tecnalia-France, Montpellier, France.*

[b] *Aix Marseille Univ, CNRS, IRD, INRA, Coll France, CEREGE, Aix-en-Provence, France.*

[d] *OSUG-FAME, UMS 832 CNRS-Univ. Grenoble Alpes, F-38041, Grenoble, France*

CORRESPONDING AUTHOR FOOTNOTE:

Perrine Chaurand. E –mail : chaurand@cerege.fr

DECLARATION OF INTEREST: NONE

HIGHLIGHTS.

- Release of Ce due to matrix photo-degradation
- 2 distinct phases of release
- The release of 1 wt.% of the initial Ce mass appears as a realistic scenario for outdoor exposure of ca. 3.5 years
- The presence of CeO_2 nanoparticles in the acrylic stain modifies the behavior of the matrix toward weathering.

ABSTRACT.

The release of CeO_2-bearing residues during the weathering of an acrylic stain enriched with CeO_2 nanomaterial designed for wood protection (Nanobyk brand additive) was studied under two different scenarios: *(i)* a standard 12-weeks weathering protocol in climate chamber, that combined condensation, water spraying and UV-visible irradiation and *(ii)* an alternative accelerated 2-weeks leaching batch assay relying on the same weathering factors (water and UV), but with a higher intensity of radiation and immersion phases. Similar Ce released amounts were evidenced for both scenarios following two phases: one related to the removal of loosely bound material with a relatively limited release, and the other resulting from the degradation of the stain, where major release occurred. A non-linear evolution of the release with the UV dose was evidenced for the second phase. No stabilization of Ce emissions was reached at the end of the experiments. The two weathering tests led to different estimates of long-term Ce releases, and different degradations of the stain. Finally, the photo-degradations of the nanocomposite, the pure acrylic stains and the Nanobyk additive were compared. The incorporation of Nanobyk into the acrylic matrix significantly modified the response of the acrylic stain to weathering.

KEYWORDS. Aging of nanomaterials, engineered nanomaterials (ENM) release, photo-degradation, polymer nanocomposites, acrylic stain.

CAPSULE.

The weathering of a nano-CeO_2-enriched acrylic stain caused a multi-regime non-linear Ce release, accompanied by mutually dependent aging of both the matrix and the CeO_2-nanomaterial.

MANUSCRIPT TEXT.

Introduction

The necessity to better estimate and characterize the release of engineered nanomaterials (ENMs) from products has been pointed out repeatedly these past years (Caballero-Guzman and Nowack, 2016; Mackevica and Foss Hansen, 2016; Reijnders, 2009; Som et al., 2010). Real exposure assessments are indeed still hampered by the difficulty to detect and quantify ENMs in complex natural environments (Szakal et al., 2014). While models have been developed to compensate the lack of direct measurements, they often have to rely on oversimplifications and extrapolations in order to estimate the exposure resulting from ENMs release (Caballero-Guzman and Nowack, 2016), which lowers their reliability. A more accurate determination of ENMs flows at all stages of the products lifecycle is then required.

The use phase is particularly challenging, as uncontrolled releases of ENMs can result from consumer handling or aging of the products. Such releases cannot be easily determined in the everyday life. Then the simulation of relevant aging scenarios under controlled conditions at the lab-scale appears as a good option.

The release of ENM during the use phase will depend on the nanoproduct category. For instance, the release from liquid suspensions is inherent to use and will be around 100%, while the release from solid nanocomposites is more difficult to predict. Solid nanocomposites are materials constituted with a solid

matrix and ENMs that can be either deposited at the solid surface or incorporated in the bulk as filling agents (nanofiller). The release of ENM from a solid nanocomposite can proceed from the leaching of ENMs by a liquid, via desorption from the surface, dissolution, or diffusion inside the matrix (Bossa et al., 2017; Duncan and Pillai, 2015). But it can also arise from the degradation of the solid matrix itself, caused by a mechanical action (Bressot et al., 2017) or (photo)chemical reactions (Duncan, 2015).

Products with an outdoor application will be especially exposed to photo-degradations due to weathering processes. The weathering of solid nanocomposites has been the focus of several studies since the release of TiO_2 nanoparticles from facades was evidenced for the first time by Kaegi *et al.* (Kaegi et al., 2008). Outdoor weathering setups with rain collectors were developed and allowed measuring the release of silver nanoparticles from an acrylic white paint (Kaegi et al., 2010) or from wood protective stains (Künniger et al., 2014) under natural conditions. However, such realistic scenarios required long-term exposures and many other groups preferred short-term lab-scale artificial weathering, that are pre-validated to correlate with material degradation CEN standards (Podgorski et al., 2003). In the past decade, short-term artificial weathering has been performed on paint (Wang and Nowack, 2018), stains (Shandilya et al., 2015), cement (Bossa et al., 2017; Wohlleben et al., 2011) and plastic nanocomposites (Fernández-Rosas et al., 2016; Neubauer et al., 2017; Nguyen et al., 2010; Wohlleben et al., 2017), either using homemade setups (Al-Kattan et al., 2013; Bernard et al., 2011; Olabarrieta et al., 2012; Pellegrin et al., 2009) or commercial climate chambers (Fiorentino et al., 2015; Hirth et al., 2013; Vilar et al., 2013; Zuin et al., 2013). Although a variety of weathering protocols have been tested, they most often included the exposure of the material to an artificial light source, simulating the full solar spectra (Busquets-Fité et al., 2013; Wohlleben et al., 2013), or restricted to its UV-part (Al-Kattan et al., 2013; Chin et al., 2004; Fiorentino et al., 2015). It was often combined with an exposure to water such as controlled relative humidity (Nguyen et al., 2010), periodic condensation (Fiorentino et al., 2015) or water spraying phases (Fernández-Rosas et al., 2016), representative for humidity, dew or rain, respectively. Depending on the groups, different methods were applied for release assessment. Some focused on quantifying the spontaneous release of ENMs during the

91 weathering assays, using collectors to gather particles detached by gravity (Nguyen et al., 2011), or run-
92 off waters from spraying (Al-Kattan et al., 2015; Busquets-Fité et al., 2013). However, this involved
93 large volumes of water (up to 5000L (Al-Kattan et al., 2013)). As an alternative, some authors
94 implemented external release assessment, with (Hirth et al., 2013; Hsu and Chein, 2007) or without
95 additional mechanical stress (Zuin et al., 2013) (e.g. shaking, sonication, abrasion). Although these
96 different approaches were found successful, the diversity of protocols and setups made difficult the
97 comparison between studies, the understanding of the mechanisms and laws governing ENMs release.
98 Recently, efforts were made towards harmonization of the experimental protocols, in the framework
99 of large pilot interlaboratory studies (Wohlleben et al., 2017, 2014). They converged towards
100 weathering procedures in climate chambers with or without periodic water spraying, and external
101 release assessment. This harmonized protocol yielded contrasted results, depending on the nature on the
102 material: UV-resistant polymers such as polyethylene led to minimal release, while epoxy resins
103 experienced strong degradations under UV, entailing an accumulation of the ENMs at the surface, and
104 eventually their release. A comparative study on a wide range of nanocomposites estimated that release
105 rates from different matrices were spreading across 5 orders of magnitude while the impact of the
106 nanofiller itself on the release rate was limited to one order of magnitude (Wohlleben and Neubauer,
107 2016). It was then proposed that matrix degradability determined to a large extent the response of a
108 nanocomposite to weathering and the ENMs release behavior.
109 In this study, we focused on a single polymer matrix and analyzed the impact of the addition of a
110 nanomaterial to its weathering. We used an acrylic stain that offers a good resistance to UV (Chiantore
111 et al., 2000; Forsthuber et al., 2013) and is commonly employed for wood protection. It was enriched
112 with a CeO_2 nanomaterial, which acts as a UV-absorber and brings an additional protection to the stain.
113 We studied the weathering of this nanocomposite to answer two questions: i) is there a potential for
114 release of the nanomaterial upon aging of a UV-resistant matrix ? ii) is the weathering of the acrylic
115 matrix modified in presence of the CeO_2 nanomaterial? In addition, we characterized a parameter rarely
116 addressed in details i.e. the evolution of the release rate with the UV irradiation. Two artificial

weathering procedures were applied: a standard 12-weeks weathering protocol in a climate chamber, that combined condensation, water spraying and UV-visible irradiation, close to the harmonized protocol mentioned above; and an alternative accelerated 2-weeks batch assay applying the same weathering factors (water and UV), but with a higher intensity of radiation. In both experiments, the nanocomposite was weathered along with the reference stain without CeO_2 addition, in order to evaluate the impact of the nanomaterial on the aging. Surface degradations were monitored as an indicator for weathering. The release of Ce (as dissolved and/or particulate fraction) was quantified with short time steps (e.g. 24h to 72h), to analyze the release dynamics during weathering and relate it to the degradations of the stain surface. Finally the physico-chemical transformation of the nanomaterial within the stain with weathering duration was characterized to give an insight into aging mechanisms.

Material and methods

Materials

An acrylic stain commercialized by Castorama under one of its brand (Lasure Intérieur- Extérieur casto') was chosen for this study. It was deposited in three layers, on larch substrates, freshly sanded with 180 grain paper, observing 2-hours drying between successive layers and 24h final drying.

Two groups of samples were prepared. In the first group (called n-CeO_2), the stain was enriched with citrate-coated CeO_2 nanoparticles, to improve UV filtering. For this, a commercial suspension (Nanobyk-3810) was added to the stain at 7wt.%, and this mix was applied to the upper face (*i.e.* exposed face) of the substrate sample (Figure 1). The characterization and aging of Nanobyk additive was done previously (Auffan et al., 2014). Lateral and lower faces were coated with the stain alone to protect the wood substrate during weathering.

In parallel, a second group of samples (called ACR) was painted on all faces with the Ce-free stain. It was used as a reference to evaluate the impact of ENM addition on the aging of the stain.

For the weathering experiments in the climate chamber (Suntest samples), larch blocks of 27 x 27 x 13 mm were cut. They were weighed before and immediately after the application of each layer of stain. Taking into account a 18% CeO_2 content for Nanobyk additive (Tella et al., 2014), the amount of CeO_2 deposited on each sample (upper face) was calculated, and is reported in Table 1.

For batch experiments, the stain deposit was made on a larger piece of wood (600 x 35 x 11 mm), cut afterwards into 35 x 35 x 11 mm blocks. Lateral faces were covered with Ce-free stain after cutting. This method resulted in a less accurate determination of CeO_2 content, as final samples could not be weighed individually. CeO_2 surface concentration and stain density were then assessed based on the assumption that batch samples exhibited the same final CeO_2 content (wt.%) as Suntest samples.

Table 1. Exposed surface, dry stain mass and density, mean CeO_2 mass deposited on samples, and resulting CeO_2 content (wt.%) and surface concentration. Standard deviation is reported in parenthesis. On batch samples, no data was available regarding the final mass of the stain. An equivalent CeO_2 final content (wt.%) to Suntest samples was assumed and CeO_2 surface concentration, stain density and stain mass after drying were calculated based on this assumption (in italics).

	Suntest		**Batch**	
	n-CeO_2	ACR	n-CeO_2	ACR
Exposed surface (mm^2)	729	729	1225	1225
Stain mass after drying (mg)	38 (18)	48 (36)	*40 (20)*	*27 (22)*
Stain density ($g.m^{-2}$)	52 (24)	70 (47)	*33 (17)*	*22 (18)*
Deposited CeO_2 (mg)	1.5 (0.2)	-	1.8 (0.3)	-
Final CeO_2 content (wt.%)	4.5 (1.5)	-	*4.5 (1.5)*	-
CeO_2 surface concentration ($mg.m^{-2}$)	2089 (273)	-	1481 (289)	-

Artificial weathering

Two artificial weathering procedures, based on a succession of dry irradiation and immersion or water spraying phases, were tested. The two sets of experiments were both built on a cycle of 7 days applying the same weathering factors but they were not designed to be compared in term of Ce release and stain degradation. The first one was performed in a climate chamber Suntest XLS+ (Atlas

Material testing Solutions, Germany) for 12 weeks. It combined dry UV irradiation phases with water spraying events to simulate as much as possible a long-term "realistic" scenario. The weathering program was inspired from a standardized protocol (NF EN 927-6, 2006) specific to wood stains, but it was adapted to quantify in details Ce releases and release rates with the UV irradiation and to differentiate Ce release as dissolved Ce from particulate Ce.

A second simplified and accelerated protocol was developed for a 2-weeks batch experiment (batch test). It was designed to provide complementary information on the light effect by comparing release from illuminated samples and non-illuminated samples (dark samples). The purpose of this protocol was to determine whether the release behavior of a solid nanocomposite could be estimated with a short-term experiment.

Weathering in the climate chamber Suntest XLS+:

As described in standard NF EN 927-6, the weathering program was based on weekly cycles repeated for 12 weeks. The weekly weathering cycle started with a 24h condensation, performed in a homemade setup outside the climate chamber (Figure S1, Supplementary Content). Then, ACR and n-CeO_2 samples were introduced inside the Suntest XLS+ and alternatively exposed to Xe lamp and Milli-Q water spraying for the rest of the week. Adaptations to the standard protocol were made, in order to quantify Ce releases and monitor their evolution during weathering. First of all, the volume of water sprayed was strongly reduced, by lowering the spraying frequency from 30 minutes every 180 minutes (NF EN 927-6), to four 20 minutes events, distributed over the week as described by Figure 1a. The water flowing at the surface of samples during spraying phases was collected in order to evaluate Ce releases induced by weathering. To do so, groups of 6 samples, representing a total exposed surface of 4374 mm^2, were placed inside 800mL glass beakers. Raised and slanted PTFE holders were used, to avoid immersion and water stagnation at the sample surface. A total of five beakers (3 with n-CeO_2 and 2 with ACR) holding 6 samples were fitted inside the climate chamber, arranged on a rotating plate (PL SPP 2 with PMMA plate Ø 300mm, MG Industries, France) to ensure

187 homogenous spraying on all the samples (Figure 1c). Each beaker was weighed before and after each
188 "rain" event to determine the exact volume of water received by the samples. In average 145 mL ± 42
189 mL water were collected in one beaker during the 20 minutes spraying, which corresponded to a mean
190 L/S ratio (rain volume/exposed stain mass) around 500 - 600 for each rain event. The cumulative L/S
191 ratio at the end of the experiment was between 24000 and 30000 (depending on the beaker). Water
192 sampling from these lixiviates was carried out 3 times a week as indicated by the asterisks in Figure
193 1a for ICP-MS analysis. More details on the water sampling protocol can be found in Supplementary
194 content.
195 During irradiation phases, the intensity of radiation was set to 65J.m^{-2}.s^{-1} (300nm-400nm) at chamber
196 floor, resulting in an effective UV intensity of 91 J.m^{-2}.s^{-1} at the elevated position of samples.
197 Complementary with UV dose, irradiance in the 300 nm – 800nm range was measured once a week
198 with an external radiometer MacSolar (SOLARC, Germany) and was found to be around 500 J.m^{-2}.s^{-1}
199 at the sample surface. The chamber temperature was around 30°C (max 36.6°C) during dry irradiation
200 phases and 21°C (max 30.5°C) during water spraying, while black body temperature (BST panel) was
201 measured respectively at 52°C (max 64.4°) and 21°C (max 32.9°C). An additional measurement of
202 the temperature at sample surface during an irradiation phase indicated a value of *ca* 36°C.
203 At the end of each weekly cycle, one n-CeO_2 and one ACR sample were withdrawn from the
204 experiment and replaced by fresh samples. The degradation of the stain could then be followed week
205 after week. After 12 weeks, 1000 mm precipitations and a UV dose of 513 MJ.m^{-2} (2826 MJ.m^{-2} in
206 the 300 nm – 800 nm range) were accumulated by the oldest samples. In France, such precipitations
207 and irradiance are usually reached in 8-12 months depending on the area(INES Education, n.d.;
208 "Météo France - Météo et Climat," n.d.)
209 <u>Batch weathering:</u>
210 In this test, a higher intensity of radiation (i.e. radiant exposure in the 300-800 nm range) was used
211 and full immersion of the sample was substituted to water spraying in order to accelerate weathering.

Immersion was also selected because it could be implemented more easily. The detailed experimental protocols are described below.

Batch weathering was based on a weekly cycle as during the Suntest experiments. It alternated dry irradiation phases with 5 immersions, distributed over the week as shown in Figure 2. During immersions, stained samples (ACR and n-CeO2 samples, n=3 for each condition) of 35 x 35 x 11 mm, with an exposed surface of 1225 mm^2, were placed in separate polypropylene (PP) beakers and submerged for 1.5h in 150mL Milli-Q water. One beaker without sample was also set up for blank. Constant magnetic stirring ensured a good homogenization of the leachate. pH and conductivity were measured before and after each immersion. At the end of immersion, a 20mL-aliquot was extracted for ICP-MS analysis. It was compensated with an equivalent volume of Milli-Q water to maintain a constant L/S ratio (immersion volume/stain mass) of 3750 during the whole experiment. Between two immersions, samples were withdrawn from the PP beakers and exposed to a 400W HPI-T Plus Metal Halide lamp (Philips, France, see Figure S2 for emission spectra). Beakers with leachate were covered and maintained in the dark to avoid leachate evolution until the next immersion. The distance of the sample to the lamp was adjusted to reach a high intensity of radiation. Mean irradiance at sample surface was measured at 105 $J.m^{-2}.s^{-1}$ for UV range (290nm-390nm) and 1300 $J.m^{-2}.s^{-1}$ for the 300nm-800 nm range, with a PCE-UV34 radiometer (PCE Ibérica S.L., Spain.) and MacSolar radiometer, respectively.

The experiment was reproduced for 2 consecutive weeks resulting in a UV dose of 97 $MJ.m^{-2}$ (1367 $MJ.m^{-2}$ in the 300 nm-800 nm range) at the end of the assay. Sample temperature alternated between 44°C during irradiation phase and 27°C during immersions.

The same weathering experiment of 2 weekly cycles was also performed in the dark (immersion step without irradiation) to investigate the influence of light on the degradation of the stain and nanomaterials release. The experimental setup and the weekly weathering cycle are detailed in Figure 2.

Quantification of Ce release

Ce concentration in lixiviates of both experiments was analyzed by ICP-MS (Nexion 300, Perkin Elmer, France) after acidification at 2,5% HNO_3 (Ultrapure NORMATON 67%) following Ce isotope (^{140}Ce). In the Suntest experiments, 20mL of sub-sample were filtrated at 10kDa (using Amicon 8050 unit with cellulose membrane) before acidification in order to determine dissolved fraction of Ce in the lixiviates.

Alteration of the nanocomposite due to weathering

The degradation of the stains was estimated based on the detection of defects. Three phenomena defined in standard NF EN 927-6 were monitored: blistering, flaking and cracking. Blistering is defined as a lifting of the stain from the underlying surface, which appears as bubbles or blisters in the paint, usually caused by heat, moisture or a combination of both. It can eventually lead to peeling of the stain if not corrected. Cracking indicates splitting of the paint film through at least one coat, leading to failure of the paint. In its early stages, the problem appears as hairline cracks; in its later stages, flaking, i.e. a peeling of the paint from the underlying surface in the form of flake, can occur.

The observation of defects was made by optical microscopy at magnification x5 and x10, on a Leica DM RXP microscope. ISO standards 4628-1(2003) (ISO 4628-1, 2003), 4628-2(2003) (ISO 4628-2, 2003), 4628-4(2003) (ISO 4628-4, 2003) and 4628-5(2003) (ISO 4628-5, 2003) were used as references to rate defect size and density. Grades for defects density and size are detailed in supporting information (tables S4 and S5).

Moreover, the oxidation state of Ce inside the stain was characterized before and after weathering, as an indicator for the alteration of CeO_2 nanomaterial. To this end, a thin laminate of the exposed face of Suntest samples was cut and analyzed by X-ray Absorption Near-Edge Spectroscopy (XANES) at the Ce-L_3 edge (5723 eV). Acquisition was made in the fluorescence mode (Canberra Ge-solid-state detector) on the CRG-FAME BM30B beamline at the ESRF (Grenoble, France). The beam size was 100µm x 300µm. Ce^{III}-oxalate and the commercial additive Nanobyk-3810, which contained only

263 $Ce^{IV}O_2$ nanoparticles as determined previously (Auffan et al., 2014), were used as Ce^{III} and Ce^{IV}
264 reference compounds, respectively. Each spectrum was at least the sum of two scans. XANES data were
265 processed using an IFEFFIT software package(Ravel and Newville, 2005). Linear Combination Fits
266 were performed in order to determine the relative Ce^{III} and Ce^{IV} contents.
267

268 ## Results

269 *Dynamics of Ce release*

270 Ce releases measured after water spraying events in the Suntest and immersions of batch experiments
271 are reported in Figure 3a and Figure 4a. Data were plotted as a function of the UV dose. A table giving
272 the equivalence between weathering time in weeks, UV dose and irradiation in the 300 nm – 800 nm
273 range for both experiments is presented in Table S3.

274 For the Suntest experiments, Ce was detected in all lixiviates obtained from n-CeO_2 samples, while it
275 was below the ICP-MS detection limit (DL< 0.1ng.g^{-1}) for the majority of ACR samples. Occasional
276 levels above DL probably result from a contamination and cannot be considered as representative for a
277 release of Ce from the stain matrix.

278 Besides the strong initial release (327 ± 28 µg.m^{-2}), the measured Ce releases varied from a few µg.m^{-2}
279 to ~200 µg.m^{-2}. This corresponded to Ce concentrations between 0.1 and 5 µg.L^{-1} in "rain" waters. In
280 Figure 3a, strong fluctuations are observed between consecutive time points. They are due to the
281 modulations of the weekly weathering cycle in Suntest experiments, that imposed different irradiation
282 times (22h, 44h or 72h) or number of water spraying events (1 or 2) between two sampling events
283 (Figure 1a). In order to reduce this variation and better observe the general trend, Ce releases of Suntest
284 experiment were integrated over the weekly cycle (Figure 3b). Two different regimes of emissions can
285 be distinguished. During the four first weeks of weathering (total UV irradiation ≤ 155 MJ.m^{-2}) Ce
286 releases are erratic with a rather decreasing trend. After 5 weeks, weekly emissions start increasing.

Their magnitude increases with cumulative UV irradiation, and no stabilization is reached at the end of the experiment (12 weeks, 513 $MJ.m^{-2}$).

The chemical analysis of the Suntest samples filtrated at 10kDa (Figure 3b, light blue) shows that Ce is released in the form of both particulate and dissolved species. The calculated Dissolved/Total Ce ratio varies strongly during the four first weeks of experiments, but after 155 $MJ.m^{-2}$ (4 weeks), it oscillates between 0.3 and 0.5 with a mean value of 0.4. CeO_2 nanoparticles in the additive initially consist in pure Ce^{IV} (cerianite CeO_2) (Auffan et al., 2014) and are considered to be poorly soluble in aquatic media (Söhnel and Garside, 1992) . The presence of dissolved Ce in the lixiviates indicates an alteration of the nanomaterial and implies the reduction of Ce^{IV} to Ce^{III} (more soluble at pH 6).

For batch experiment (Figure 4a), a release of 75-250 $\mu g.m^{-2}$ of Ce was detected directly after immersion 1 regardless of the irradiation regime (dark or light). Cerium release did not exceed background levels from 32 $MJ.m^{-2}$ to 46 $MJ.m^{-2}$ (immersion 4), then increased for n-CeO_2 samples exposed to light, while they remained below the DL for samples kept in the dark. The first measurable releases at 46 $MJ.m^{-2}$ were around 0.08 $mg.m^{-2}$ of Ce, then kept increasing to reach 1.3 ± 0.4 $mg.m^{-2}$ of Ce at 97 $MJ.m^{-2}$. This trend was disturbed only by a strong release event at 77 $MJ.m^{-2}$ (2.9 ± 1.8 $mg.m^{-2}$ of Ce, immersion 1, week 2), which is probably the result of the longer irradiation period of 72h at the beginning of the new cycle. Combined with the absence of Ce release from dark samples after immersion 1, this shows a clear correlation between exposure to sunlight and Ce emissions. Once again, no stabilization in Ce release was observed at the end of the experiment, which is consistent with the trend measured for the Suntest experiments at higher cumulated UV doses.

The two aging scenarios express a very similar behavior, with two distinct phases for Ce release. The initial phase (phase I) showed an overall decreasing trend with time and no clear dependency on light. In the second phase (phase II) emissions increased with weathering and are light-dependent. No plateau in Ce release was observed at the end of both assays.

Ce releases cumulated over the duration of the experiments were plotted in Figure 3c and Figure 4b. They confirmed the similar trends observed for both experiments. At the end of the aging experiments,

313 the total Ce release reached 2.8 ± 0.3 mg.m^{-2} for the Suntest and 6.0 ± 2.4 mg.m^{-2} for the batch assay. In
314 both cases, this represented less than 1wt.% of the initial Ce mass (~0.16wt.% for Suntest samples,
315 ~0.5wt.% for batch samples). A strong initial release was measured during the first rain event of the
316 Suntest experiments (327 ± 28 µg.m^{-2} of Ce) accounting for 12% of total Ce emissions. The initial
317 release was much lower in batch test, (< 0.1 µg of Ce) accounting for only 1.3% of the total Ce
318 emissions. For the two tests, most of the Ce release took place in the second part of the experiment
319 (phase II), representing 73% and 98% of Ce emissions, for the Suntest protocol (after 155 MJ.m^{-2}) and
320 batch experiment (after 46 MJ.m^{-2}), respectively.
321 In order to get an insight on Ce release for longer weathering durations, release curves obtained in the
322 two experiments were fitted by a second order polynomial law. Fitting parameters are reported in Table
323 2. Fits were extrapolated to assess the irradiation necessary to reach the release of 1%, 10% or 100%
324 release of the initial Ce mass in our specific experimental conditions (i.e. for a given type and thickness
325 of stain). For the Suntest protocol, 1wt.% of the initial Ce amount is predicted to be released after 1250
326 MJ.m^{-2}, 10% after 3800 MJ.m^{-2} and 100% after 11800 kWh.m^{-2}. According to the Solar Radiation Data
327 ("SoDa - Web Services," n.d.), the annual UV dose corresponding to the area of Marseille in France is
328 around 350 MJ.m^{-2}. Based on this data, the release of 1% of the initial Ce mass corresponds to 3.5 years
329 of aging of the stain. However, the release of 10wt.% or 100wt.% of the Ce present in the stain would
330 require 10 and 33 years, respectively. The fit of batch data leads to very different values, with 1% of
331 total Ce mass being released after 130 MJ.m^{-2}, 10% after 355 MJ.m^{-2} and 100% after 1070 MJ.m^{-2}.
332 These values correspond to outdoor exposures of 4 months, 1 year and 3 years in the south of France.
333
334 **Table 2.** Parameters of the polynomial fit of release curves. $y = m_0 + m_1*x + m_2*x^2$.

Experiment	**m_0**	**m_1**	**m_2**	**R^2**
Suntest	0.8171	- 0.0024	1 x 10^{-5}	0.997
Batch	- 0.158	- 0.0479	1.1 x 10^{-3}	0.995

335

Figure 5 shows the evolution of defect density and size for ACR and n-CeO_2 stains observed for the two aging scenarios. Before weathering, the samples were generally free of defects. Isolated flakes were present on a few samples but cracking and blistering were not observed. The samples that were weathered in the dark did not develop any defect (not shown). On the contrary, defects appeared at the surface of samples that were exposed to light (Figure S4). The batch aging protocol induced blistering for both Ce-enriched or Ce-free stain, but no cracking nor flaking was observed (Figure 5c and d). Similar blisters sizes and densities were measured for ACR and n-CeO_2 samples, with a growing magnitude as aging proceeded. For ACR samples weathered in Suntest XLS+, defects mainly took the shape of flakes and cracks (Figure 5a). Blistering was rarely observed. Defects appeared at a very early stage of the experiments. However their density remained rather low (mainly grade 1, as defined in ISO 4628-2, 4628-4 and 4628-5) and their size ranked mostly S1 (*i.e.* = only visible under magnification x10) or S2 (*i.e.* = incipiently visible with normal and corrected vision) on some occasions (indicated by a star symbol). Neither defect density nor size showed a significant evolution with the UV dose, confirming the good resistance of this material to weathering.

A totally different pattern emerged for n-CeO_2 samples. Their surface remained rather free of defects during the four first weeks of experiment, showing a good initial resistance to weathering. Nevertheless, after 155 $MJ.m^{-2}$ (dotted line in Figure 5b), defects started multiplying. As ACR samples, n-CeO_2 samples displayed cracks under microscopic magnification (x10) but their density reached higher grades. Flaking was absent from the nanocomposite surface after weathering, but contrary to the reference material, dense and large blisters became visible. No significant variations in defect sizes were observed with aging, but the density was clearly higher after 4 weeks weathering (155 $MJ.m^{-2}$), correlated with the change in Ce release regime (Figure 3b).

Cracks are the defects most frequently reported for acrylic stains weathered under both artificial (Aloui, 2006; Irmouli et al., 2012; Kielmann and Mai, 2016; Olsson et al., 2014; Popescu and Simionescu, 2013) and natural conditions (De Windt et al., 2014; Olsson et al., 2014). They can sometimes lead to

flaking, but blistering is usually not expected. This scenario matches well the observations made on ACR samples of our Suntest experiment but deviates from what was observed for the rest of samples. During batch testing, blistering was developed in a similar way for Ce-enriched or Ce-free stain. This effect could then find an origin in the experimental protocol itself, where repeated immersions could favor water penetration and entrapment at the wood/stain interface. After Suntest weathering (and periodic condensation phases), n-CeO_2 samples showed a significant blistering, which was absent from the surface of ACR samples (Ce-free stain);

In addition to wood stain degradation, the oxidation state of Ce inside the stain was monitored as an indicator for the alteration of the CeO_2 nanomaterial. XANES spectra of the Nanobyk additive and the non-weathered n-CeO_2 sample are given in Figure 6. They exhibit two peaks (double white line) at ~ 5728 eV and ~ 5735 eV, corresponding respectively to the final states $2p4f^15d^1L$ and $2p4f^05d^2$ of Ce^{IV} (Dexpert et al., 1987; Finkelstein et al., 1992) . Both match perfectly showing that CeO_2 nanoparticles were not altered by their incorporation into the stain and its deposition onto a wood substrate. After 12 weeks of weathering following the Suntest protocol (513 MJ. m^{-2} UV dose), the double white line characteristic of Ce^{IV} states is still visible on the XANES spectra. However a third peak appeared at ~5724 eV that is the absorption energy of the Ce^{III} reference compound. $Cerium^{III}$ oxalate is also plotted in Figure 6 and presents a single white line, corresponding to the $2p_{3/2}$ / $4f^15d$ electronic transition (Takahashi et al., 2002), at ~5724 eV. Consequently, we assume that part of the Ce initially present in the stain as Ce^{IV} was then reduced to Ce^{III} during weathering. Linear Combination Fits (LCF) were performed on the derivatives of XANES spectra to determine the relative Ce^{IV} and Ce^{III} contents. The results are reported in Table 3 for three different locations on the sample. On average, a Ce^{III} content of 38% ± 4% was found.

Table 3. Results of the Linear Combination Fits (LCF) performed on the derivatives of XANES spectra measured at three different spots of an n-CeO_2 sample weathered for 12 weeks in Suntest XLS+ (513 $MJ.m^{-2}$). The error on the calculated Ce^{IV} and Ce^{III} content is ± 10%

n-CeO_2 12 weeks	**Ce^{IV}**	**Ce^{III}**	**R**	**chi^2**
Spot 1	73%	42%	0.012981	0.03407
Spot 2	79%	33%	0.010084	0.02433
Spot 3	75%	38%	0.015139	0.03815

Discussion

Release of Ce

The release of Ce from an acrylic matrix enriched with a CeO_2 nanomaterial (Nanobyk additive) was evidenced with our two weathering protocols. Far from being a negligible phenomenon, Ce emissions from 2 to 200 $\mu g.m^{-2}$ were measured for each rain event from the beginning of the Suntest experiment. After 46 $MJ.m^{-2}$, Ce release ranging from 0.08 to 2.9 $mg.m^{-2}$ was also systematically observed during the immersions of the batch test. The residual release detected for samples maintained in the dark in batch experiment indicates that the exposure to UV (and visible) irradiation is the driving force of the release. Water certainly acts as a vector removing degradation debris from the sample surface, but did not induce weathering in the absence of UV. Combined to UV, it very likely contributed to accentuate the weathering via hydrolytic reactions, as suggested by Wohlleben et al. in the case of polyamide (Wohlleben et al., 2014). Cumulated over the experiment, Ce release caused by water spraying events during Suntest testing reached *ca*. 3 $mg.m^{-2}$. Recently, harmonized weathering protocols have been proposed, using external release measurements (Wohlleben et al., 2017) that would exclude such spontaneous release from their assessment, resulting in an inaccurate determination of the released mass.

Dynamics of Ce release

The evolution of release as a function of the UV irradiation was thoroughly analyzed in our two weathering scenarios. They revealed dynamic release processes that could similarly be divided in two distinct phases and presented common features in both experiments. The first phase (phase I) showed a decreasing trend with time, similarly to what was described by other authors for paints (Al-Kattan et al., 2013; Kaegi et al., 2010). As no clear dependency on light exposure was found, the release mechanism is certainly a wash off of loosely bound material from the surface. Unlike in the above-cited studies, in this experiment, the initial phase was followed by a second one, where Ce emissions increased for irradiated samples and kept growing until the end of the tests. The exposure to UV-visible radiation and the dose received by the samples appeared as key parameters in that phase. In particular, phase II showed a significant accentuation of Ce release with increasing exposure to UV radiation. We postulate then, that release was a consequence of the photo-degradation of the stain, as already witnessed for epoxy (Nguyen et al., 2011) or polyamide (Fernández-Rosas et al., 2016). In both experiments, it was found that the release measured in the second phase accounted for more than 70% of the total Ce release (73% in Suntest and 98% in batch test). Therefore the release due to photo-degradation largely predominates over the release of loose material in this study. No stabilization of Ce release was reached at the end of our experiments. Increased Ce emissions are expected, if weathering proceeds on the same trend, but they could also accentuate and accelerate if matrix aging gets worse. Indeed, previous work already showed that strong damages occurred on commercial photocatalytic stains after 7 months lab weathering, with a direct impact on the amount and the form of TiO_2 nanoparticles released during abrasion processes (Shandilya et al., 2015). Prolonged laboratory tests or higher radiant exposures are necessary to determine the long-term release behavior.

It is interesting to highlight that the release rates determined in phase II did not follow a linear trend, and were fitted instead by a 2^{nd} order function. Until now, release studies often provided as result a single value of release rate. This is appropriate when release observes a constant or linear trend, as reported for nano-SiO_2 in acrylic paints (Al-Kattan et al., 2015) or epoxy (Nguyen et al., 2010). However, a recent review (Koivisto et al., 2017) pointed out that release may not always be linearly

proportional to the UV dose. The authors introduced a relation to describe the release due to UV radiation as follow:

$$R = a \times D^b$$

Where R is the release rate in $mg.m^{-2}$, D the UV irradiation energy in $MJ.m^{-2}$, and a and b are fitting parameters. A b factor around 1, implying linearity between the release rate and UV dose, was determined on four occasions for release data found in the literature, but values of $b \neq 1$ were predominant. Our results support a non-linear release function in the case of the n-CeO_2 nanocomposite, but could not be fitted satisfactorily by a power law. This may be due to the fact that the release function proposed by Koivisto *et al*. is analogous to the Schwarzschild's law, and describes photo responses resulting from irradiation (Martin et al., 2003). In our experiments an additional factor of degradation was present in the form of water, which may cause a divergence from the power law. Besides, we identified two distinct regimens of Ce release, similarly to what was observed for Si release from 5 wt. % nano-SiO_2 epoxy composite (Sung et al., 2015) and polyurethane nanocomposite (Jacobs et al., 2016).

It suggests that different processes may be at stake in ENM release and emphasizes the need for investigating the dynamics of release more carefully.

Long-term release estimates

Surprisingly, despite very different weathering conditions, our experimental aging protocols displayed a very good agreement in their overall release tendencies (i.e. stain degradation and Ce release). However, significant deviations appeared with a more quantitative analysis Extrapolation of the data indeed led to totally different estimates of the UV doses necessary to reach 1wt.%, 10wt.% or 100wt.% release of the Ce initially present in the material. In the Suntest experiment, the release of 1% of the initial Ce mass appeared as a realistic scenario for an outdoor exposure of *ca*.3.5 years. The release of 10% of the initial Ce puts the aging well beyond the typical recommended 5 year lifetime of an outdoor wood stain, and the 100% release of Ce would even take 33 years. On the other hand the extrapolation of batch data (i.e.

460 implying repeated full immersion of the samples) concluded that 1% release should be achieved after a
461 few months, 10% short after 1 year and 100% after about 3 years. All these durations lied within the
462 lifetime of the stain (ca. 5 years) and a 100% release could then be expected based on this experiment.

463

464 *Stain degradation due to weathering*

465 In addition to release quantification, the alteration of the stain caused by weathering was
466 characterized, based on the occurrence of defects (blisters, flakes or cracks) at the sample surface. It
467 unveiled another divergence between the two weathering protocols, in the defects produced on the
468 stains. Blistering was predominant on both ACR and n-CeO_2 samples of the batch testing, while it was
469 rarely observed under natural circumstances. This suggested that the applied weathering conditions may
470 be unrealistic and questioned the reliability of the release assessment in that case. On the contrary, the
471 weathering of ACR stains in the Suntest XLS+, showing slight cracking and flaking, was consistent
472 with what is usually observed under natural conditions (De Windt et al., 2014; Olsson et al., 2014). This
473 confirmed both the good resistance of acrylic stains to weathering and the realistic character of the
474 Suntest experiment.

475 Contrary to ACR samples, the n-CeO_2 samples weathered with the Suntest protocol showed a
476 densification of their defects after 155 $MJ.m^{-2}$. It coincided with the increase of Ce release, reinforcing
477 the hypothesis that Ce emissions of phase II resulted from a degradation of the stain. It also suggested
478 that there is a relationship between defect formation and release. A high density of defects was observed
479 on the Suntest samples and the release rate at 110 $MJ.m^{-2}$ was around 0.7 $mg.m^{-2}$. For the batch samples,
480 the density and size of surface defects remained lower, but they displayed an almost ten times higher
481 release rate at 97 $MJ.m^{-2}$: 6 $mg.m^{-2}$. Therefore we conclude that Ce release was not a direct
482 consequence of the formation of cracks or blisters. We rather think that these are two outcomes of the
483 same degradation phenomenon. If the correlation between the formation of defects and release can be
484 confirmed on other systems, defects could however serve as an indicator for release in the future.

485 The higher cracking density measured for n-CeO_2 samples with respect to the pure acrylic stain, may
486 result from a stiffening of the film, due to dense Ce. The n-CeO_2 samples also developed blisters that
487 were not observed on the ACR samples (CeO_2-free stain). This suggests that the incorporation of CeO_2
488 nanoparticles to the acrylic matrix modified its response to weathering.
489
490 *Aging of CeO_2 nanomaterial inside the stain*
491 Finally the presence of dissolved Ce was evidenced in lixiviates. X-ray absorption spectroscopy proved
492 that the reductive dissolution of the CeO_2 nanomaterial started in the stain, leading to the release of
493 dissolved Ce^{III} in the lixiviates. The initial CeO_2 nanoparticles experienced a transformation during the
494 weathering of the nanocomposite, resulting in the release of a material significantly different from the
495 pristine CeO_2 nanoparticles. In the past years, literature reviews established that ENM release from a
496 solid nanocomposite often took the form of nanomaterial embedded in matrix fragments (Froggett et al.,
497 2014) behaving differently than the pristine ENM (Al-Kattan et al., 2014). Here, we bring new elements
498 suggesting that even if free ENMs were released, they may have experienced transformations during the
499 weathering process, affecting their fate, their transport, their interactions with organisms and thus
500 modify their behavior in the environment compared to pristine material. Strikingly, the aging of the
501 Nanobyk additive in water under UV radiation brought into light an alteration of the CeO_2 nanoparticles
502 (Auffan et al., 2014). However it consisted in a reorganization of Ce atoms at the nanoparticle surface
503 and in that case, no reduction of Ce^{IV} to Ce^{III} was detected. In this study, a different response to aging
504 was observed for the Nanobyk additive incorporated to the acrylic stain. On the other hand the acrylic
505 stain also displayed a different weathering behavior with or without embedded nanomaterial. This
506 advocates for the need of studying nanocomposites as novel materials, with potentially different
507 responses than their separate compounds.

508 **Conclusions**

509 The dynamics of Ce release from a CeO_2-acrylic nanocomposite designed for wood protection was
510 investigated under short- and middle-term assays. It revealed two different regimes of release, as well as
511 a non-linear relationship between the release rate and UV irradiation, highlighting that release
512 phenomena cannot always be properly described by a single release rate value. Efforts should then be
513 made to better characterize the dynamics of release from nanocomposites and help to improve the
514 accuracy of ENM flow models (Wang and Nowack, 2018).

515 In this work, two weathering scenarios (a realistic middle-term experiment in climate chamber and a
516 simplified short-term batch test), specifically designed to monitor the evolution of the release rates with
517 time and UV doses were tested. They displayed a good agreement regarding the occurrence of dual
518 release regimes. In absence of a release plateau during the experiments, polynomial fits of the release
519 curves were used to provide estimates of long-term release. The similarity in general release trends
520 between the two tests showed here some limits, as they led to very different estimates of Ce releases.
521 Indeed, calculations indicate that after 3.5 years, 100 wt.% of the initial Ce will be released based on the
522 batch experiment vs 1 wt.% in the Suntest experiment). .

523 The two protocols also produced different surface defects on the stains. In particular the defects
524 observed on batch samples were pointed out as unrealistic, while the Suntest protocol mimicked natural
525 weathering more faithfully. This supports the reliability of the release rates determined with this
526 procedure and makes it a good candidate for standardized tests. The good agreement of batch
527 experiment on the overall release tendency, suggests that it could rather serve as a screening test, to
528 evaluate the release behavior of a nanocomposite. Systematic testing on a range of materials is
529 necessary before such a use could be validated.

530 Based on the Suntest experiment the release of 1% of the initial Ce mass during the lifetime of the
531 stain appears as realistic. However longer experiments are needed to confirm this estimate. An
532 intensification of the matrix degradations could indeed induce the loss of the acrylic polymer structure,
533 resulting in a third phase of release.

Finally, the incorporation of CeO_2 nanoparticles into the acrylic matrix has been shown to modify the response of the stain to weathering while the CeO_2 nanomaterial experienced a transformation that was not expected based on previous weathering experiments. The weathering of a nanocomposite cannot be decomposed as the weathering of two isolated parts. Synergistic effects can arise between the matrix and its nanomaterial, making the study of the weathering of nanocomposites necessary.

ACKNOWLEDGMENT.

The authors thank TECNALIA Foundation for funding the weathering studies under its internal Nanotechnology Programme. This work was also supported by the project on Sustainable Nanotechnologies (SUN) that received funding from the European Union Seventh Framework Programme (FP7/2007−2013) under grant agreement no. 604305. The project leading to this publication has received funding from "Excellence Initiative" of Aix-Marseille University A*MIDEX, a French "Investissements d'Avenir" program, through its associated Labex SERENADE (n° ANR-11-LABX-0064). We acknowledge the European Synchrotron Radiation Facility for provision of synchrotron radiation facilities and we would like to thank the FAME BM30b team for assistance in using their beamline.

551 REFERENCES.

552

553 Al-Kattan, A., Wichser, A., Vonbank, R., Brunner, S., Ulrich, A., Zuin, S., Arroyo, Y., Golanski, L.,
554 Nowack, B., 2015. Characterization of materials released into water from paint containing nano-SiO2.
555 Chemosphere 119, 1314–1321. https://doi.org/10.1016/j.chemosphere.2014.02.005

556 Al-Kattan, A., Wichser, A., Vonbank, R., Brunner, S., Ulrich, A., Zuin, S., Nowack, B., 2013. Release
557 of TiO2 from paints containing pigment-TiO2 or nano-TiO2 by weathering. Env. Sci Process Impacts
558 15.

559 Al-Kattan, A., Wichser, A., Zuin, S., Arroyo, Y., Golanski, L., Ulrich, A., Nowack, B., 2014. Behavior
560 of TiO2 Released from Nano-TiO2-Containing Paint and Comparison to Pristine Nano-TiO2. Environ.
561 Sci. Technol. 48, 6710–6718. https://doi.org/10.1021/es5006219

562 Aloui, F., 2006. Rôle des absorbeurs UV inorganiques sur la photstabilisation des systèmes bois-finition
563 transparente (Doctorat). Université Henri Poincaré - Nancy 1, Vandoeuvre les Nancy.

564 Auffan, M., Masion, A., Labille, J., Diot, M.-A., Liu, W., Olivi, L., Proux, O., Ziarelli, F., Chaurand, P.,
565 Geantet, C., Bottero, J.-Y., Rose, J., 2014. Long-term aging of a CeO2 based nanocomposite used for
566 wood protection. Environ. Pollut. 188, 1–7. https://doi.org/10.1016/j.envpol.2014.01.016

567 Bernard, C., Nguyen, T., Pellegrin, B., Holbrook, R., Zhao, M., Chin, J., 2011. Fate of grapheme in
568 polymer nanocomposite exposed to UV radiation. J Phys Conf Ser 304.

569 Bossa, N., Chaurand, P., Levard, C., Borschneck, D., Miche, H., Vicente, J., Geantet, C., Aguerre-
570 Chariol, O., Michel, F.M., Rose, J., 2017. Environmental exposure to TiO2 nanomaterials incorporated
571 in building material. Environ. Pollut. 220, 1160–1170. https://doi.org/10.1016/j.envpol.2016.11.019

572 Bressot, C., Manier, N., Pagnoux, C., Aguerre-Chariol, O., Morgeneyer, M., 2017. Environmental
573 release of engineered nanomaterials from commercial tiles under standardized abrasion conditions.
574 Journal of Hazardous Materials 322 276-283. https://doi.org/10.1016/j.jhazmat.2016.05.039

575 Busquets-Fité, M., Fernandez, E., Janer, G., Vilar, G., Vázquez-Campos, S., Zanasca, R., Citterio, C.,
576 Mercante, L., Puntes, V., 2013. Exploring release and recovery of nanomaterials from commercial
577 polymeric nanocomposites. J Phys Conf Ser 429.

578 Caballero-Guzman, A., Nowack, B., 2016. A critical review of engineered nanomaterial release data:
579 Are current data useful for material flow modeling? Environ. Pollut. 213, 502–517.
580 https://doi.org/10.1016/j.envpol.2016.02.028

581 Chiantore, O., Trossarelli, L., Lazzari, M., 2000. Photooxidative degradation of acrylic and methacrylic
582 polymers. Polymer 41, 1657–1668. https://doi.org/10.1016/S0032-3861(99)00349-3

583 Chin, J., Byrd, E., Embree, N., Garver, J., Dickens, B., 2004. Accelerated UV weathering device based
584 on integrating sphere technology. Rev. Sci. Instrum. 75. https://doi.org/10.1063/1.1808916

585 De Windt, I., Van den Bulcke, J., Wuijtens, I., Coppens, H., Van Acker, J., 2014. Outdoor weathering
586 performance parameters of exterior wood coating systems on tropical hardwood substrates. Eur. J.
587 Wood Wood Prod. 72, 261–272. https://doi.org/10.1007/s00107-014-0779-7

588 Dexpert, H., Karnatak, R.C., Esteva, J.-M., Connerade, J.P., Gasgnier, M., Caro, P.E., Albert, L., 1987.
589 X-ray absorption studies of CeO 2 , PrO 2 , and TbO 2 . II. Rare-earth valence state by L III absorption
590 edges. Phys. Rev. B 36, 1750–1753. https://doi.org/10.1103/PhysRevB.36.1750

591 Duncan, T.V., 2015. Release of Engineered Nanomaterials from Polymer Nanocomposites: the Effect of
592 Matrix Degradation. ACS Appl. Mater. Interfaces 7, 20–39. https://doi.org/10.1021/am5062757

593 Duncan, T.V., Pillai, K., 2015. Release of Engineered Nanomaterials from Polymer Nanocomposites:
594 Diffusion, Dissolution, and Desorption. ACS Appl. Mater. Interfaces 7, 2–19.
595 https://doi.org/10.1021/am5062745

596 Fernández-Rosas, E., Vilar, G., Janer, G., González-Gálvez, D., Puntes, V., Jamier, V., Aubouy, L.,
597 Vázquez-Campos, S., 2016. Influence of Nanomaterial Compatibilization Strategies on Polyamide
598 Nanocomposites Properties and Nanomaterial Release during the Use Phase. Environ. Sci. Technol. 50,
599 2584–2594. https://doi.org/10.1021/acs.est.5b05727

600 Finkelstein, L.D., Postnikov, A.V., Efremova, N.N., Kurmaev, E.Z., 1992. X-ray Ce LIII absorption in
601 CeO2 and BaCeO3: experiment and interpretation on the basis of LMTO band structure calculations.
602 Mater. Lett. 14, 115–118. https://doi.org/10.1016/0167-577X(92)90186-N

603 Fiorentino, B., Golanski, L., Guiot, A., Damlencourt, J.-F., Boutry, D., 2015. Influence of paints
604 formulations on nanoparticles release during their life cycle. J. Nanoparticle Res. 17, 1–13.
605 https://doi.org/10.1007/s11051-015-2962-0

606 Forsthuber, B., Müller, U., Teischinger, A., Grüll, G., 2013. Chemical and mechanical changes during
607 photooxidation of an acrylic clear wood coat and its prevention using UV absorber and micronized
608 TiO2. Polym. Degrad. Stab. 98, 1329–1338. https://doi.org/10.1016/j.polymdegradstab.2013.03.029

609 Froggett, S.J., Clancy, S.F., Boverhof, D.R., Canady, R.A., 2014. A review and perspective of existing
610 research on the release of nanomaterials from solid nanocomposites. Part. Fibre Toxicol. 11, 17.
611 https://doi.org/10.1186/1743-8977-11-17

612 Hirth, S., Cena, L., Cox, G., Tomovic, Z., Peters, T., Wohlleben, W., 2013. Scenarios and methods that
613 induce protruding or released CNTs after degradation of nanocomposite materials. J Nanopart Res 15.
614 https://doi.org/10.1007/s11051-013-1504-x

615 Hsu, L.-Y., Chein, H.-M., 2007. Evaluation of nanoparticle emission for TiO2 nanopowder coating
616 materials. J. Nanoparticle Res. 9, 157–163. https://doi.org/10.1007/s11051-006-9185-3

617 INES Education, n.d. CalSol.

618 Irmouli, Y., George, B., Merlin, A., 2012. Artificial ageing of wood finishes monitored by IR analysis
619 and color measurements. J. Appl. Polym. Sci. 124, 1938–1946. https://doi.org/10.1002/app.34797

620 ISO 4628-1, 2003. Paints and varnishes -- Evaluation of degradation of coatings -- Designation of
621 quantity and size of defects, and of intensity of uniform changes in appearance -- Part 1: General
622 introduction and designation system. International Standards Organization.

623 ISO 4628-2, 2003. Paints and varnishes -- Evaluation of degradation of coatings -- Designation of
624 quantity and size of defects, and of intensity of uniform changes in appearance -- Part 2: Assessment of
625 degree of blistering. International Standards Organization.

626 ISO 4628-4, 2003. Paints and varnishes -- Evaluation of degradation of coatings -- Designation of
627 quantity and size of defects, and of intensity of uniform changes in appearance -- Part 4: Assessment of
628 degree of cracking. International Standards Organization.

629 ISO 4628-5, 2003. Paints and varnishes -- Evaluation of degradation of coatings -- Designation of
630 quantity and size of defects, and of intensity of uniform changes in appearance -- Part 5: Assessment of
631 degree of flaking. International Standards Organization.

632 Jacobs, D.S., Huang, S.-R., Cheng, Y.-L., Rabb, S.A., Gorham, J.M., Krommenhoek, P.J., Yu, L.L.,
633 Nguyen, T., Sung, L., 2016. Surface degradation and nanoparticle release of a commercial
634 nanosilica/polyurethane coating under UV exposure. Journal of Coatings Technology and Research 13
635 5, 735-751. https://doi.org/10.1007/s11998-016-9796-2
636
637 Kaegi, R., Sinnet, B., Zuleeg, S., Hagendorfer, H., Mueller, E., Vonbank, R., Boller, M., Burkhardt, M.,
638 2010. Release of silver nanoparticles from outdoor facades. Environ. Pollut. 158, 2900–2905.
639 https://doi.org/10.1016/j.envpol.2010.06.009

640 Kaegi, R., Ulrich, A., Sinnet, B., Vonbank, R., Wichser, A., Zuleeg, S., Simmler, H., Brunner, S.,
641 Vonmont, H., Burkhardt, M., Boller, M., 2008. Synthetic TiO2 nanoparticle emission from exterior
642 facades into the aquatic environment. Environ. Pollut. 156, 233–239. https://doi.org/doi:
643 10.1016/j.envpol.2008.08.004

644 Kielmann, B.C., Mai, C., 2016. Application and artificial weathering performance of translucent
645 coatings on resin-treated and dye-stained beech-wood. Prog. Org. Coat. 95, 54–63.
646 https://doi.org/10.1016/j.porgcoat.2016.02.019

647 Koivisto, A.J., Jensen, A.C.Ø., Kling, K.I., Nørgaard, A., Brinch, A., Christensen, F., Jensen, K.A.,
648 2017. Quantitative material releases from products and articles containing manufactured nanomaterials:
649 Towards a release library. NanoImpact 5, 119–132. https://doi.org/10.1016/j.impact.2017.02.001

650 Künniger, T., Gerecke, A.C., Ulrich, A., Huch, A., Vonbank, R., Heeb, M., Wichser, A., Haag, R.,
651 Kunz, P., Faller, M., 2014. Release and environmental impact of silver nanoparticles and conventional
652 organic biocides from coated wooden façades. Environ. Pollut. 184, 464–471.
653 https://doi.org/10.1016/j.envpol.2013.09.030

654 Mackevica, A., Foss Hansen, S., 2016. Release of nanomaterials from solid nanocomposites and
655 consumer exposure assessment – a forward-looking review. Nanotoxicology 10, 641–653.
656 https://doi.org/10.3109/17435390.2015.1132346

657 Martin, J.W., Chin, J.W., Nguyen, T., 2003. Reciprocity law experiments in polymeric photo-
658 degradation: a critical review. Keyst. 2002 47, 292–311. https://doi.org/10.1016/j.porgcoat.2003.08.002

659 Météo France - Météo et Climat [WWW Document], n.d. . Météo Fr. URL
660 http://www.meteofrance.com

661 Neubauer, N., Scifo, L., Navratilova, J., Gondikas, A., Mackevica, A., Borschneck, D., Chaurand, P.,
662 Vidal, V., Rose, J., von der Kammer, F., Wohlleben, W., 2017. Nanoscale Coloristic Pigments: Upper
663 Limits on Releases from Pigmented Plastic during Environmental Aging, In Food Contact, and by
664 Leaching. Environ. Sci. Technol. 51, 11669–11680. https://doi.org/10.1021/acs.est.7b02578

665 NF EN 927-6, 2006. Paints and varnishes. Coating materials and coating systems for exterior wood.
666 Exposure of wood coatings to artificial weathering using fluorescent UV lamps and water. Association
667 Française de Normalisation.

668 Nguyen, T., Pellegrin, B., Bernard, C., Gu, X., Gorham, J.M., Stutzman, P., Stanley, D., Shapiro, A.,
669 Byrd, E., Hettenhouser, R., Chin, J., 2011. Fate of nanoparticles during life cycle of polymer
670 nanocomposites. J Phys Conf Ser 304.

671 Nguyen, T., Pellegrin, B., Bernard, C., Gu, X., Gorham, J.M., Stutzman, P.E., Shapiro, A., Byrd, E.,
672 Chin, J.W., 2010. Direct Evidence of Nanoparticle Release from Epoxy Nanocomposites Exposed to
673 UV Radiation, in: Nanotech 2010: Technical Proceedings of the 2010 NSTI Nanotechnology
674 Conference and Expo. Presented at the NSTI-Nanotech 2010, CRC Press, pp. 724–727.

675 Olabarrieta, J., Zorita, S., Peña, I., Rioja, N., Monzón, O., Benburia, P., Scifo, L., 2012. Aging of
676 photocatalytic coatings under a water flow: Long run performance and TiO2 nanoparticle release. Appl
677 Catal B Env. 182.

678 Olsson, S.K., Johansson, M., Westin, M., Östmark, E., 2014. Reactive UV-absorber and epoxy
679 functionalized soybean oil for enhanced UV-protection of clear coated wood. Polym. Degrad. Stab. 110,
680 405–414. https://doi.org/10.1016/j.polymdegradstab.2014.09.017

681 Pellegrin, B., Nguyen, T., Mermet, L., Shapiro, A., Gu, X., Chin, J., 2009. Degradation and nanoparticle
682 release of epoxy/nanosilica composites exposed to solar UV radiation. Nanotech 1.

683 Podgorski, L., Arnold, M., Hora, G., 2003. A reliable artificial weathering test for Wood Coatings.
684 Coating World 2, 39-48
685
686 Popescu, C.-M., Simionescu, B.C., 2013. Structural Study of Photodegraded Acrylic-Coated Lime
687 Wood Using Fourier Transform Infrared and Two-Dimensional Infrared Correlation Spectroscopy.
688 Appl. Spectrosc. 67, 606–613. https://doi.org/10.1366/12-06628

689 Ravel, B., Newville, M., 2005. ATHENA, ARTEMIS, HEPHAESTUS : data analysis for X-ray
690 absorption spectroscopy using IFEFFIT. J. Synchrotron Radiat. 12, 537–541.
691 https://doi.org/10.1107/S0909049505012719

692 Reijnders, L., 2009. The release of TiO2 and SiO2 nanoparticles from nanocomposites. Polym. Degrad.
693 Stab. 94, 873–876. https://doi.org/10.1016/j.polymdegradstab.2009.02.005

694 Shandilya, N., Le Bihan, O., Bressot, C., Morgeneyer, M., 2015. Emission of Titanium Dioxide
695 Nanoparticles from Building Materials to the Environment by Wear and Weather. Environ. Sci.
696 Technol. 49, 2163–2170. https://doi.org/10.1021/es504710p

697 SoDa - Web Services [WWW Document], n.d. . Sol. Radiat. Data. URL http://www.soda-pro.com/web-
698 services

699 Söhnel, O., Garside, J., 1992. Precipitation: basic principles and industrial applications. Butterworth-
700 Heinemann, Oxford [England] ; Boston.

701 Som, C., Berges, M., Chaudhry, Q., Dusinska, M., Fernandes, T.F., Olsen, S.I., Nowack, B., 2010. The
702 importance of life cycle concepts for the development of safe nanoproducts. Toxicology 269, 160–169.
703 https://doi.org/10.1016/j.tox.2009.12.012

704 Sung, L., Stanley, D., Gorham, J.M., Rabb, S., Gu, X., Yu, L.L., Nguyen, T., 2015. A quantitative study
705 of nanoparticle release from nanocoatings exposed to UV radiation. J. Coat. Technol. Res. 12, 121–135.
706 https://doi.org/10.1007/s11998-014-9620-9

707 Szakal, C., Roberts, S.M., Westerhoff, P., Bartholomaeus, A., Buck, N., Illuminato, I., Canady, R.,
708 Rogers, M., 2014. Measurement of Nanomaterials in Foods: Integrative Consideration of Challenges
709 and Future Prospects. ACS Nano 8, 3128–3135. https://doi.org/10.1021/nn501108g

710 Tella, M., Auffan, M., Brousset, L., Issartel, J., Kieffer, I., Pailles, C., Morel, E., Santaella, C.,
711 Angeletti, B., Artells, E., Rose, J., Thiéry, A., Bottero, J.-Y., 2014. Transfer, Transformation, and

712 Impacts of Ceria Nanomaterials in Aquatic Mesocosms Simulating a Pond Ecosystem. Environ. Sci.
713 Technol. 48, 9004–9013. https://doi.org/10.1021/es501641b

714 Tella, M., Auffan, M., Brousset, L., Morel, E., Proux, O., Chanéac, C., Angeletti, B., Pailles, C., Artells,
715 E., Santaella, C., Rose, J., Thiéry, A., Bottero, J.-Y., 2015. Chronic dosing of a simulated pond
716 ecosystem in indoor aquatic mesocosms: fate and transport of CeO_2 nanoparticles. Environ. Sci. Nano
717 2, 653–663. https://doi.org/10.1039/C5EN00092K

718 Vilar, G., Fernández-Rosas, E., Puntes, V., Jamier, V., Aubouy, L., Vázquez-Campos, S., 2013.
719 Monitoring migration and transformation of nanomaterials in polymeric composites during accelerated
720 aging. J Phys Conf Ser 429.

721 Wang, Y., Nowack, B., 2018. Dynamic probabilistic material flow analysis of nano-SiO2, nano iron
722 oxides, nano-CeO2, nano-Al2O3, and quantum dots in seven European regions. Environ. Pollut. 235,
723 589–601. https://doi.org/10.1016/j.envpol.2018.01.004

724 Wohlleben, W., Brill, S., Meier, M.W., Mertler, M., Cox, G., Hirth, S., von Vacano, B., Strauss, V.,
725 Treumann, S., Wiench, K., Ma-Hock, L., Landsiedel, R., 2011. On the Lifecycle of Nanocomposites:
726 Comparing Released Fragments and their In-Vivo Hazards from Three Release Mechanisms and Four
727 Nanocomposites. Small 7, 2384–2395. https://doi.org/10.1002/smll.201002054

728 Wohlleben, W., Kingston, C., Carter, J., Sahle-Demessie, E., Vázquez-Campos, S., Acrey, B., Chen, C.-
729 Y., Walton, E., Egenolf, H., Müller, P., Zepp, R., 2017. NanoRelease: Pilot interlaboratory comparison
730 of a weathering protocol applied to resilient and labile polymers with and without embedded carbon
731 nanotubes. Carbon 113, 346–360. https://doi.org/10.1016/j.carbon.2016.11.011

732 Wohlleben, W., Meier, M.W., Vogel, S., Landsiedel, R., Cox, G., Hirth, S., Tomovic, Z., 2013. Elastic
733 CNT-polyurethane nanocomposite: synthesis, performance and assessment of fragments released during
734 use. Nanoscale 5, 369–380. https://doi.org/10.1039/C2NR32711B

735 Wohlleben, W., Neubauer, N., 2016. Quantitative rates of release from weathered nanocomposites are
736 determined across 5 orders of magnitude by the matrix, modulated by the embedded nanomaterial.
737 NanoImpact 1, 39–45. https://doi.org/10.1016/j.impact.2016.01.001

738 Wohlleben, W., Vilar, G., Fernández-Rosas, E., González-Gálvez, D., Gabriel, C., Hirth, S., Frechen,
739 T., Stanley, D., Gorham, J., Sung, L.-P., Hsueh, H.-C., Chuang, Y.-F., Nguyen, T., Vazquez-Campos,
740 S., 2014. A pilot interlaboratory comparison of protocols that simulate aging of nanocomposites and
741 detect released fragments. Environ. Chem. 11, 402–418.

742 Zuin, S., Gaiani, M., Ferrari, A., Golanski, L., 2013. Leaching of nanoparticles from experimental
743 water-borne paints under laboratory test conditions. J. Nanoparticle Res. 16, 2185.
744 https://doi.org/10.1007/s11051-013-2185-1

745

746

747 FIGURES.

748

749

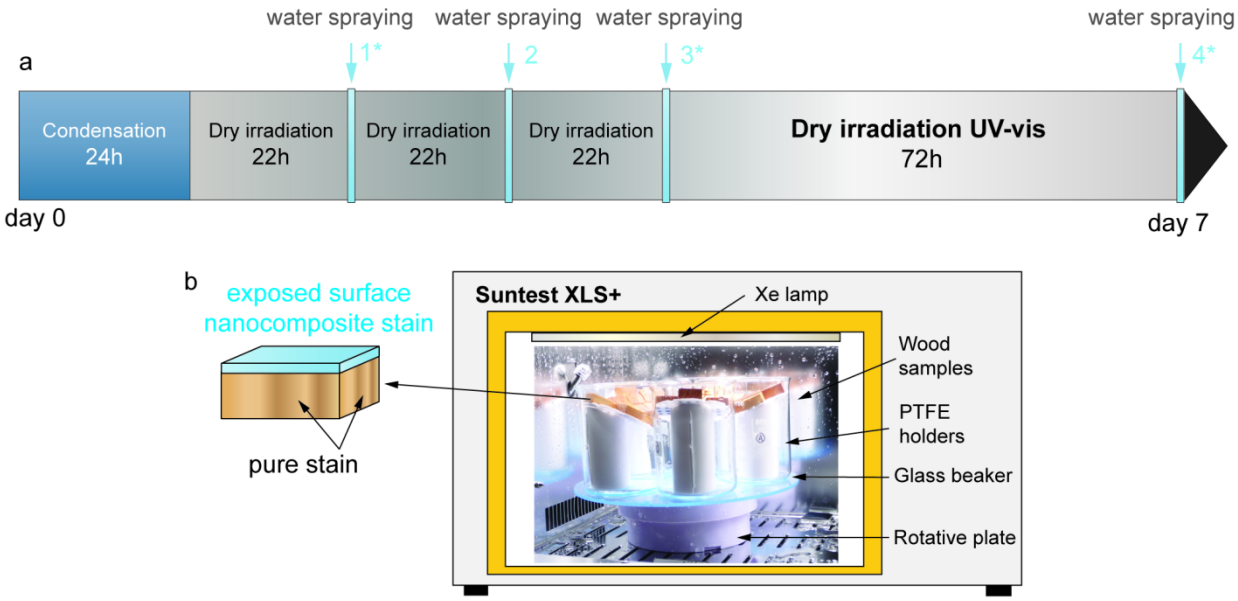

750

Figure 1. Experimental setup and procedure for weathering in climate chamber. a Weekly weathering cycle. Gray areas correspond to dry irradiation (UV-vis) phases while 20 minutes spraying events (MilliQ-water) appear in light blue. Water sampling is notified by an asterisk whenever the case. **b** Experimental setup inside Suntest XLS+ (right). Irradiation under Xe lamp and water spraying phases were applied alternatively. n-CeO_2 wood samples were coated with stain enriched with CeO_2 additive on their exposed face (= upper face), and Ce-free stain on the remaining faces, as illustrated by the left scheme. ACR samples were coated with Ce-free acrylic stain on all 6 faces.

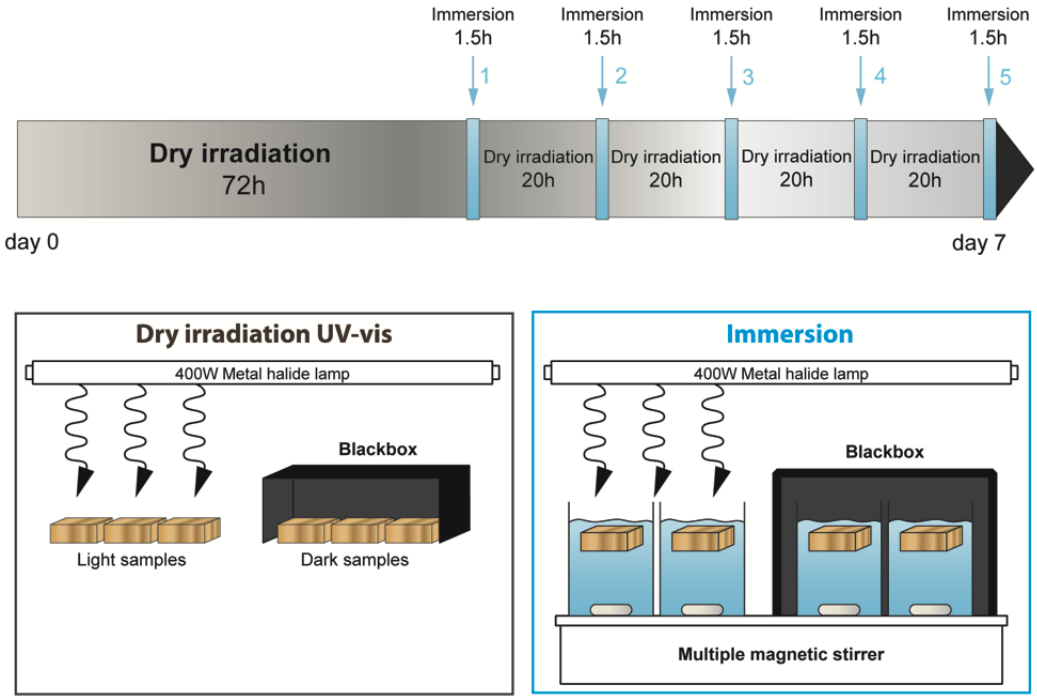

751

Figure 2. Experimental setup for batch weathering composed of successive dry irradiation and immersion phases. Left: Dry irradiation phases. Right: immersion phases. The weekly weathering cycle is described by the timeline. Gray areas correspond to dry irradiation phases while immersions (1.5h) appear in light blue. The same cycle was carried out in parallel under light exposure (irradiation + immersion) and in the dark (immersions only) for ACR and n-CeO_2 samples (n=3 for each condition). The setups for dry irradiation phases and immersion phases are illustrated in gray and blue frames respectively.

752
753

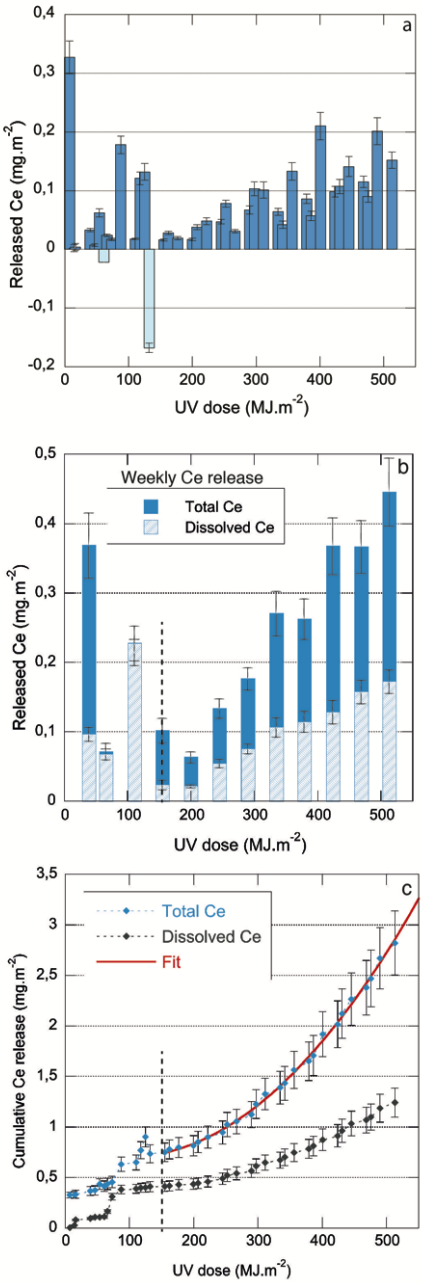

754

755

Figure 3. Ce releases taking place during water spraying of Suntest experiment. a Ce release measured between two sampling events (not cumulated). Negative releases were isolated from the series as they represent artifacts of measurement due to the sampling method. **b** Ce releases integrated over the weekly cycles of Suntest experiment. Dissolved Ce determined on samples filtrated at 10kDa is represented in light blue. The dotted line marks a change in release regime after 4 weeks weathering (155 $MJ.m^{-2}$ UV dose). **c** Cumulative release of total and dissolved Ce calculated for Suntest experiment. Ce background measured on ACR samples was included in the error bars. Ce releases of phase II were fitted by a polynomial law of the second order (in red). Fit parameters are given in Table 2.

756

757

758

759

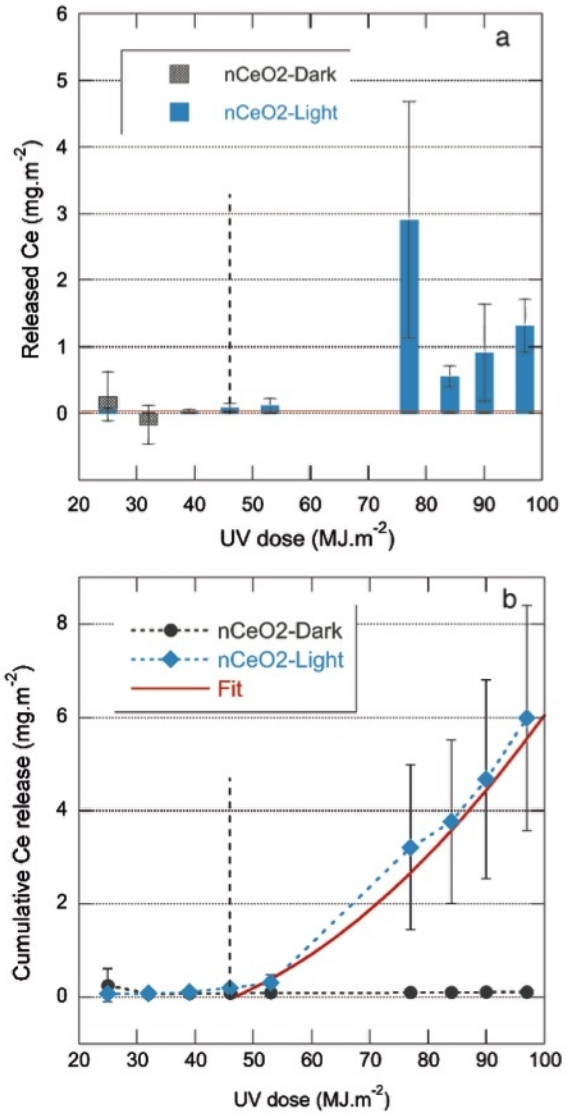

760

761

Figure 4. Ce releases taking place immersions of batch experiment. The data was averaged over three replicates. Standard deviation is represented in error bars. **a** Ce release measured for n-CeO_2 samples maintained in the dark (grey) or exposed to light (blue), during each immersion. A mean Ce background of 0.04 $mg.m^{-2}$ was estimated based on Ce level in the blank beaker (no sample) and is indicated by the red horizontal line on the graph. **b** Cumulative Ce releases calculated for batch experiment, for n-CeO_2 samples maintained in the dark (grey) and exposed to light (blue). Ce releases of phase II were fitted by a polynomial law of the second order (in red). Fit parameters are given in Table 2.

762

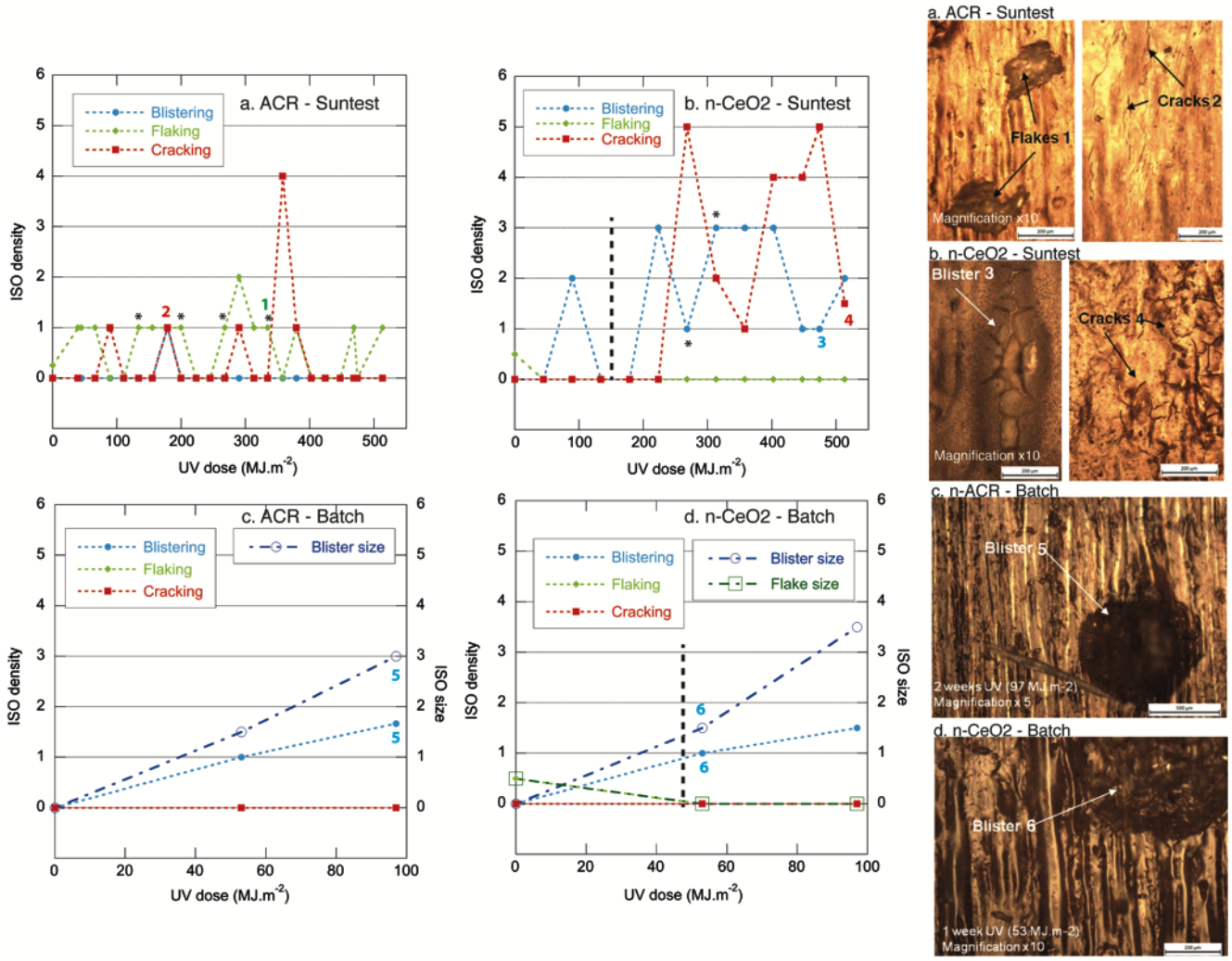

Figure 5. Assessment of stain degradation according to blistering, flaking and cracking criteria. a Defect density observed on ACR samples of Suntest experiment as a function of the UV dose. Crack size ranked S1 (only visible with magnification x10 – marked Cracks 2) for all non-zero values. For flaking most samples displayed an S1 except for the 4 points marked with a star where larger defects could be observed (marked Flakes 1) (S2, incipiently visible with normal and corrected vision). **b** Defect density observed on n-CeO_2 samples of Suntest experiment as a function of the UV dose. For blistering, most samples displayed an S3 ranking (clearly visible with normal corrected vision) (marked Blister 3), except for points indicated by a star (S2). The crack size was S1 on all samples (marked Cracks 4). **c, d** Evolution of defect density and size for **c** ACR and **d** n-CeO_2 samples exposed to light in batch experiment. The blister size was S3 (marked Blister 5 and Blister 6). No defects were observed on samples that were maintained in the dark. On **b** and **d** the dotted lines mark the onset of phase II determined from release curves. Numbers (1-6) refer to defects (cracks, flake, and blister) observed by optical microscopy (magnifications x5 and x10) and shown as example.

777

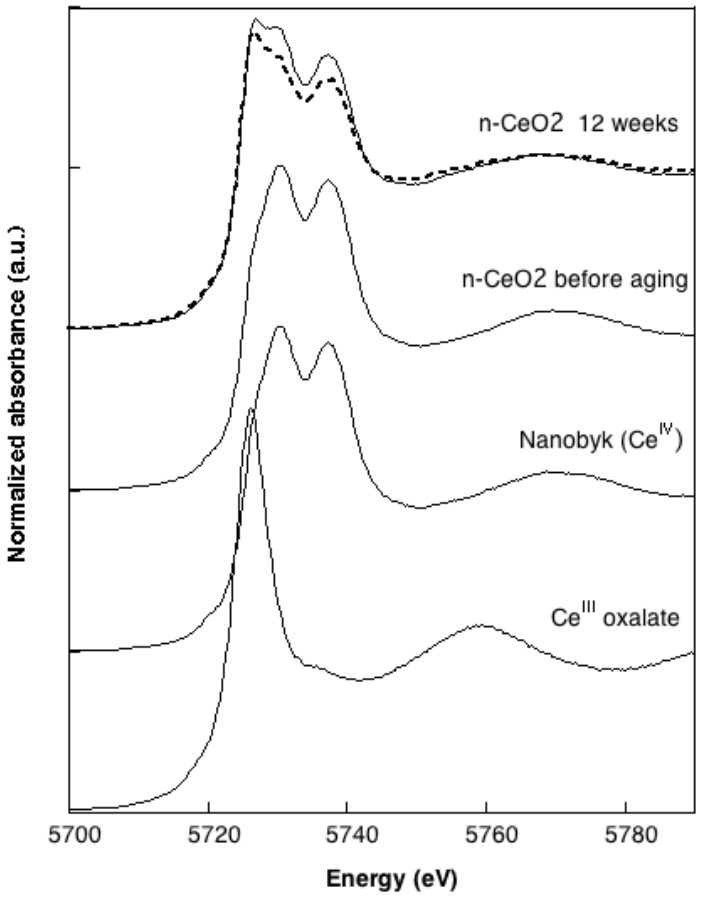

Figure 6. XANES spectra measured at the Ce L3-edge on an n-CeO_2 sample, before and after 12 weeks weathering under Suntest protocol (513 MJ.m^{-2} UV dose). The spectra obtained on the initial and weathered nanocomposite (n-CeO_2 before aging and n-CeO_2 12 weeks, respectively) are compared to those of a Ce^{III} reference (Ce^{III}-oxalate) and Nanobyk additive, serving here as Ce^{IV} reference. For the 12 weeks weathered n-CeO_2 sample, Linear Combination Fits based on Ce^{III} and Ce^{IV} reference spectra were computed (dotted line). The corresponding Ce^{III} and Ce^{IV} relative contents are reported in Table 3.

778
779
780
781
782

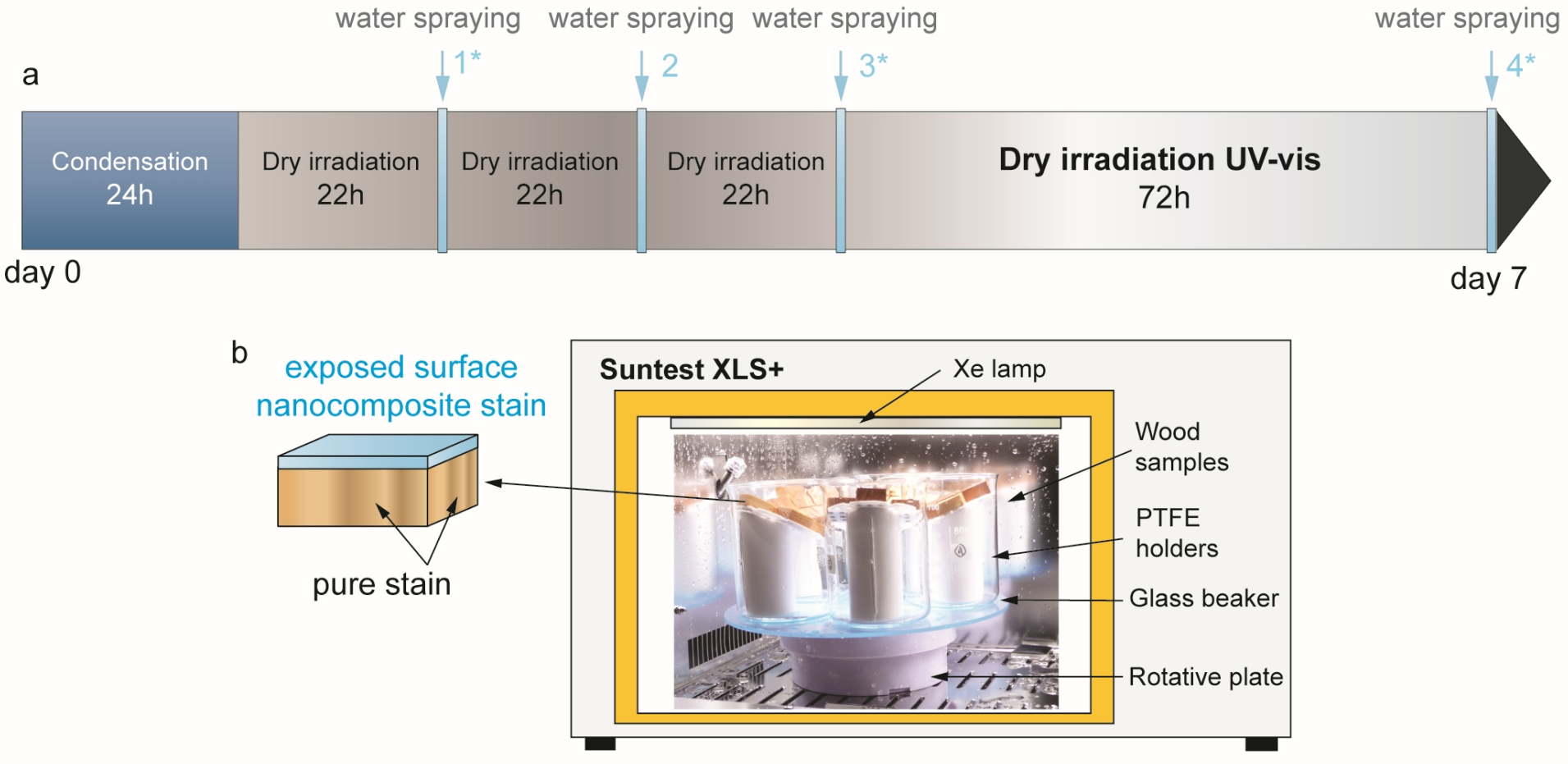
a
water spraying
1*
water spraying
2
water spraying
3*
water spraying
4*
Condensation
24h
Dry irradiation
22h
Dry irradiation
22h
Dry irradiation
22h
Dry irradiation UV-vis
72h
day 0
day 7
b
exposed surface
nanocomposite stain
pure stain
Suntest XLS+
Xe lamp
Wood
samples
PTFE
holders
Glass beaker
Rotative plate

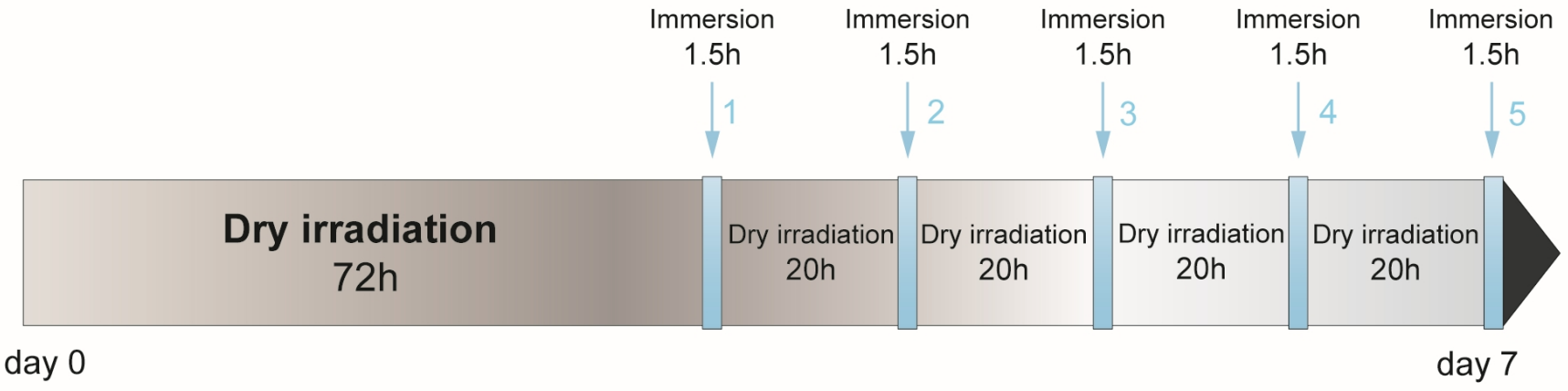
Immersion
1.5h
1
Immersion
1.5h
2
Immersion
1.5h
3
Immersion
1.5h
4
Immersion
1.5h
5
Dry irradiation
72h
Dry irradiation
20h
Dry irradiation
20h
Dry irradiation
20h
Dry irradiation
20h
day 0
day 7

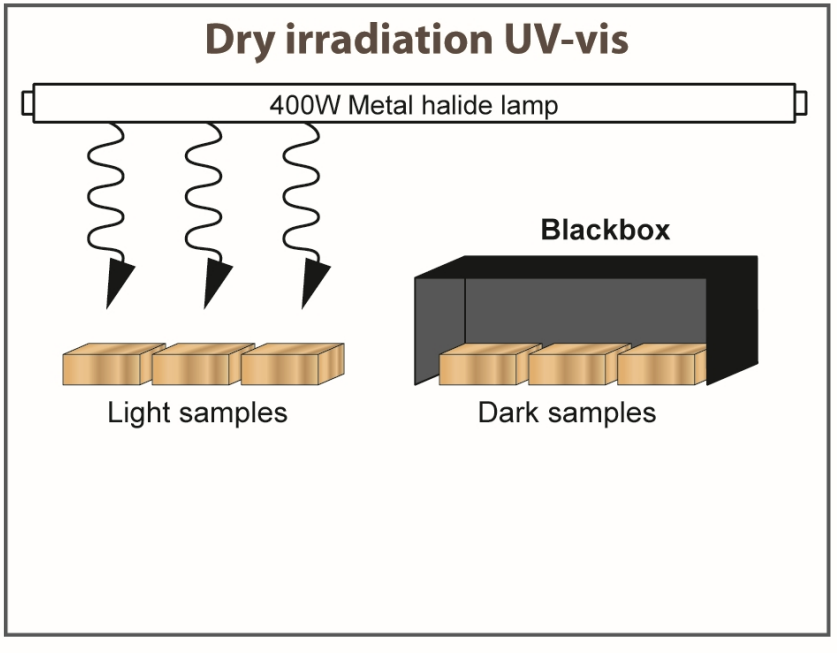
Dry irradiation UV-vis
400W Metal halide lamp
Blackbox
Light samples
Dark samples

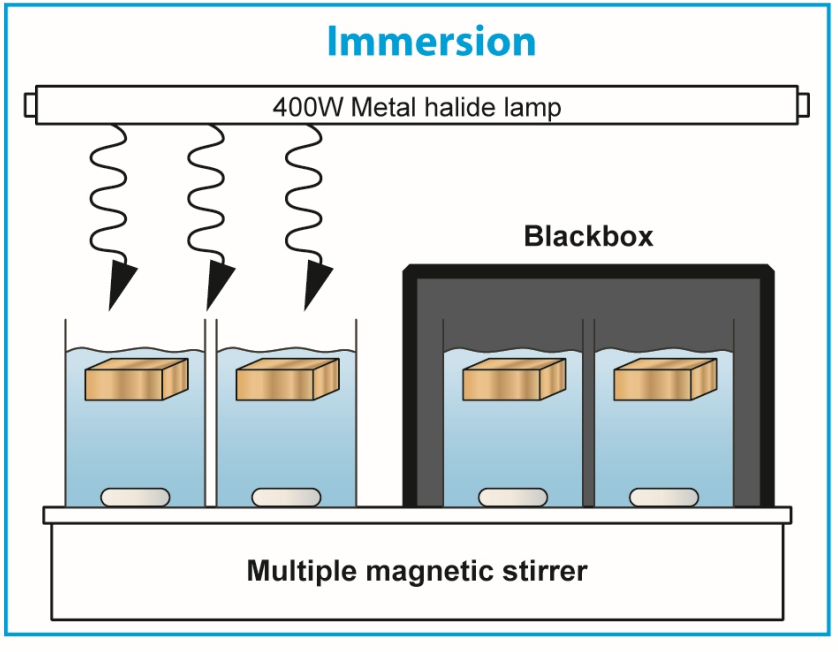
Immersion
400W Metal halide lamp
Blackbox
Multiple magnetic stirrer

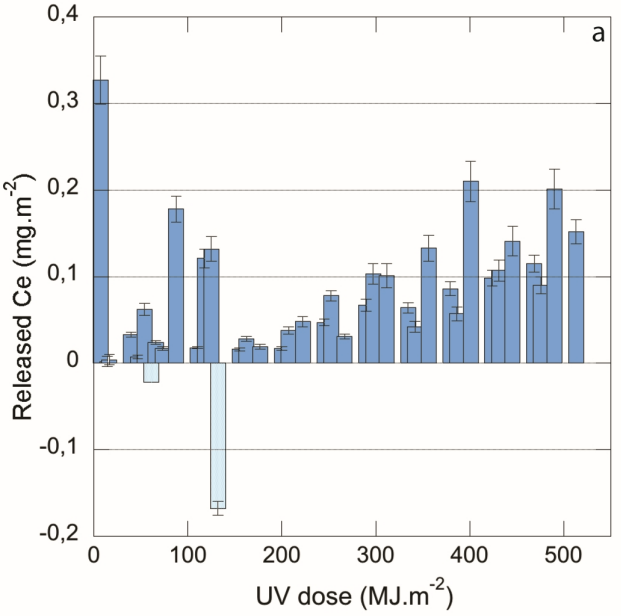
a
Released Ce (mg.m-2)
UV dose (MJ.m-2)
0,4
0,3
0,2
0,1
0
-0,1
-0,2
0
100
200
300
400
500

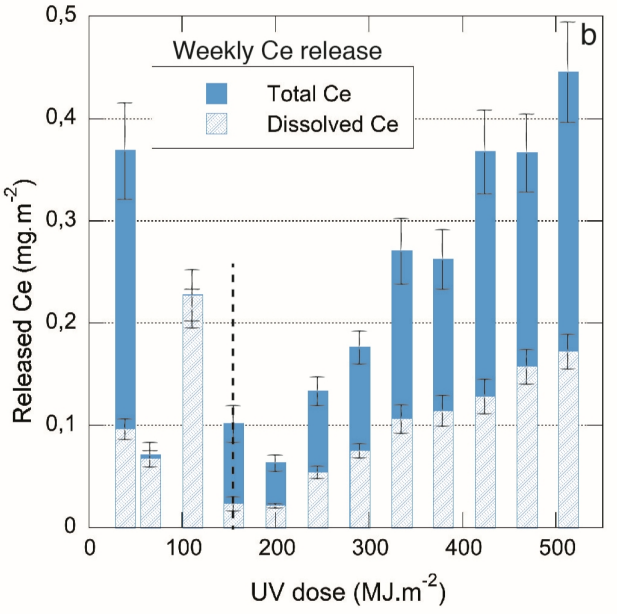
b
Weekly Ce release
Total Ce
Dissolved Ce
Released Ce (mg.m-2)
UV dose (MJ.m-2)
0,5
0,4
0,3
0,2
0,1
0
0
100
200
300
400
500

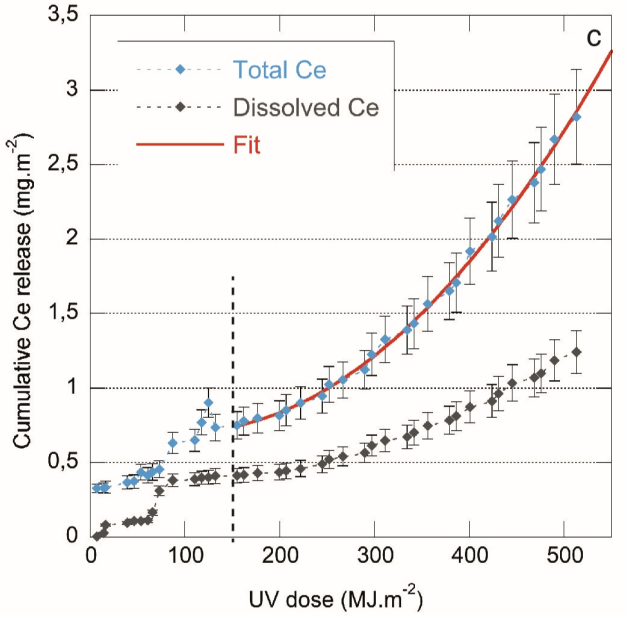
c
Total Ce
Dissolved Ce
Fit
Cumulative Ce release (mg.m-2)
UV dose (MJ.m-2)
3,5
3
2,5
2
1,5
1
0,5
0
0
100
200
300
400
500

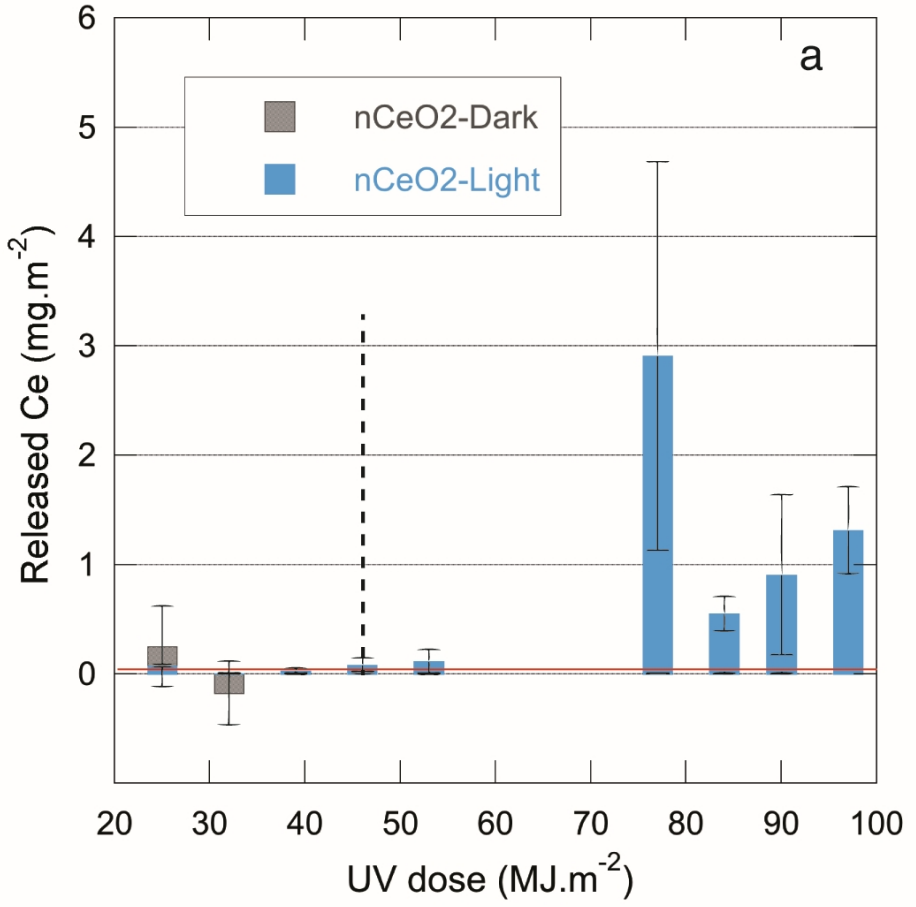
a
nCeO2-Dark
nCeO2-Light
Released Ce (mg.m-2)
UV dose (MJ.m-2)
0
1
2
3
4
5
6
20
30
40
50
60
70
80
90
100

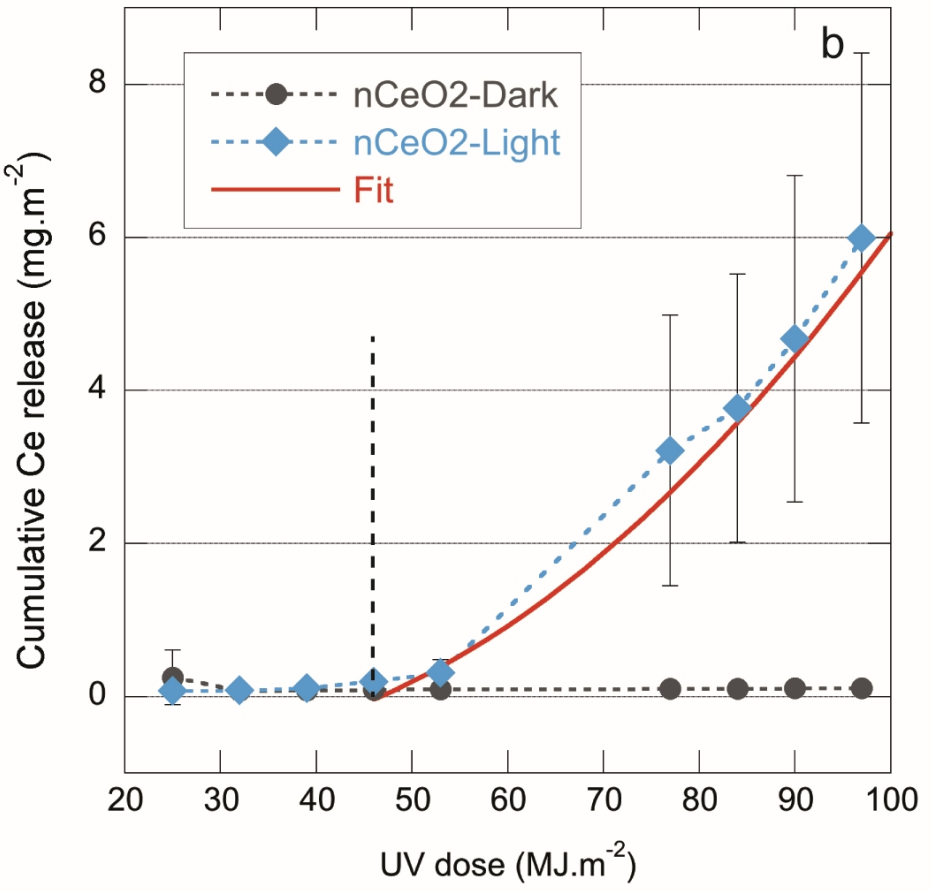
b
nCeO2-Dark
nCeO2-Light
Fit
Cumulative Ce release (mg.m-2)
UV dose (MJ.m-2)
0
2
4
6
8
20
30
40
50
60
70
80
90
100

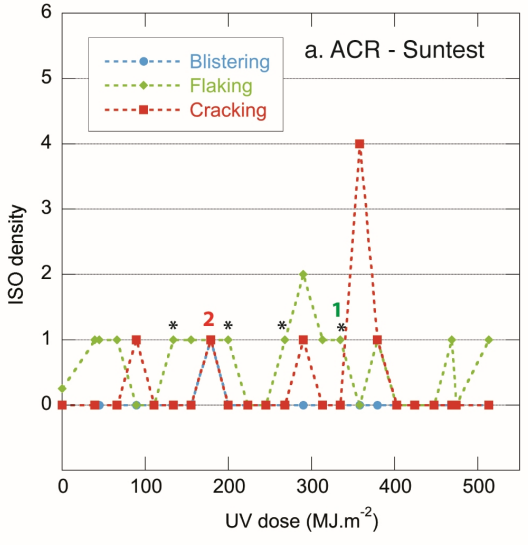
a. ACR - Suntest
Blistering
Flaking
Cracking
ISO density
UV dose (MJ.m-2)
1
2

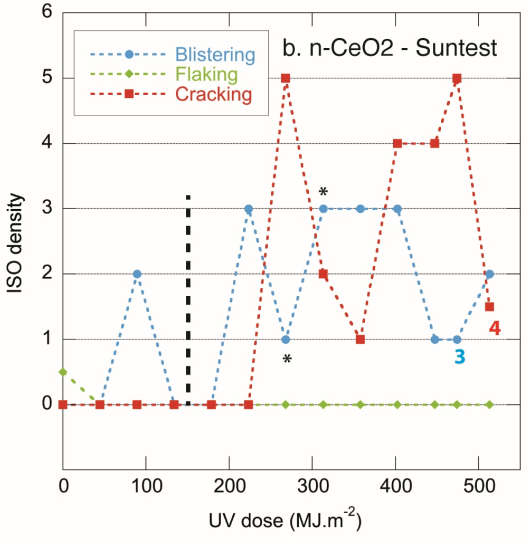
b. n-CeO2 - Suntest
Blistering
Flaking
Cracking
ISO density
UV dose (MJ.m-2)
3
4

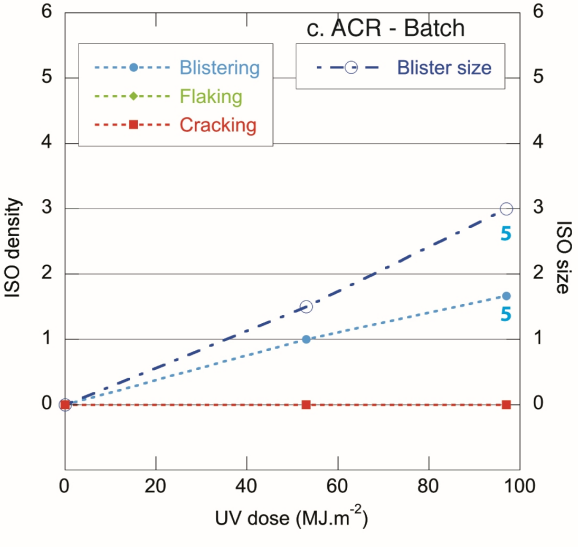
c. ACR - Batch
Blistering
Flaking
Cracking
Blister size
ISO density
ISO size
UV dose (MJ.m-2)
5

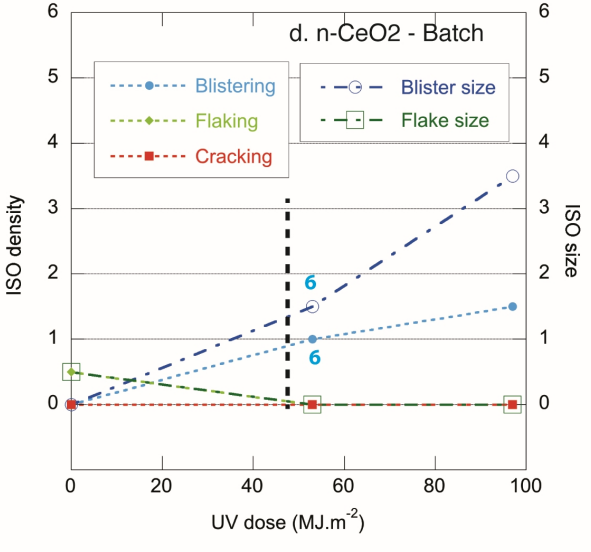
d. n-CeO2 - Batch
Blistering
Flaking
Cracking
Blister size
Flake size
ISO density
ISO size
UV dose (MJ.m-2)
6

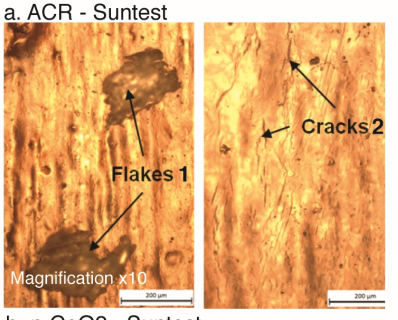
a. ACR - Suntest
Flakes 1
Cracks 2
Magnification x10

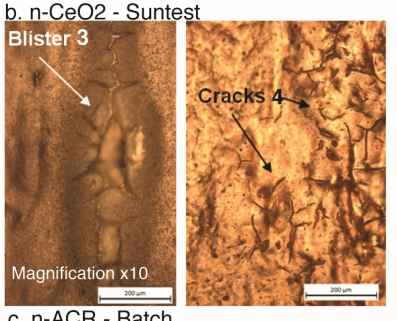
b. n-CeO2 - Suntest
Blister 3
Cracks 4
Magnification x10

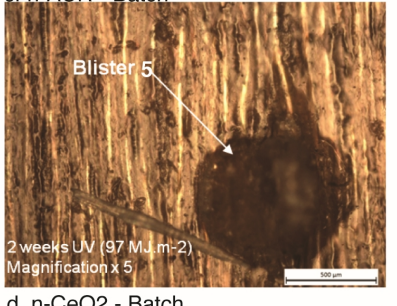
c. n-ACR - Batch
Blister 5
2 weeks UV (97 MJ.m-2)
Magnification x 5

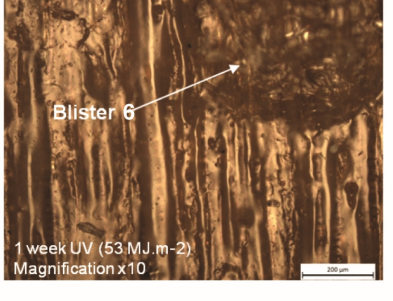
d. n-CeO2 - Batch
Blister 6
1 week UV (53 MJ.m-2)
Magnification x10

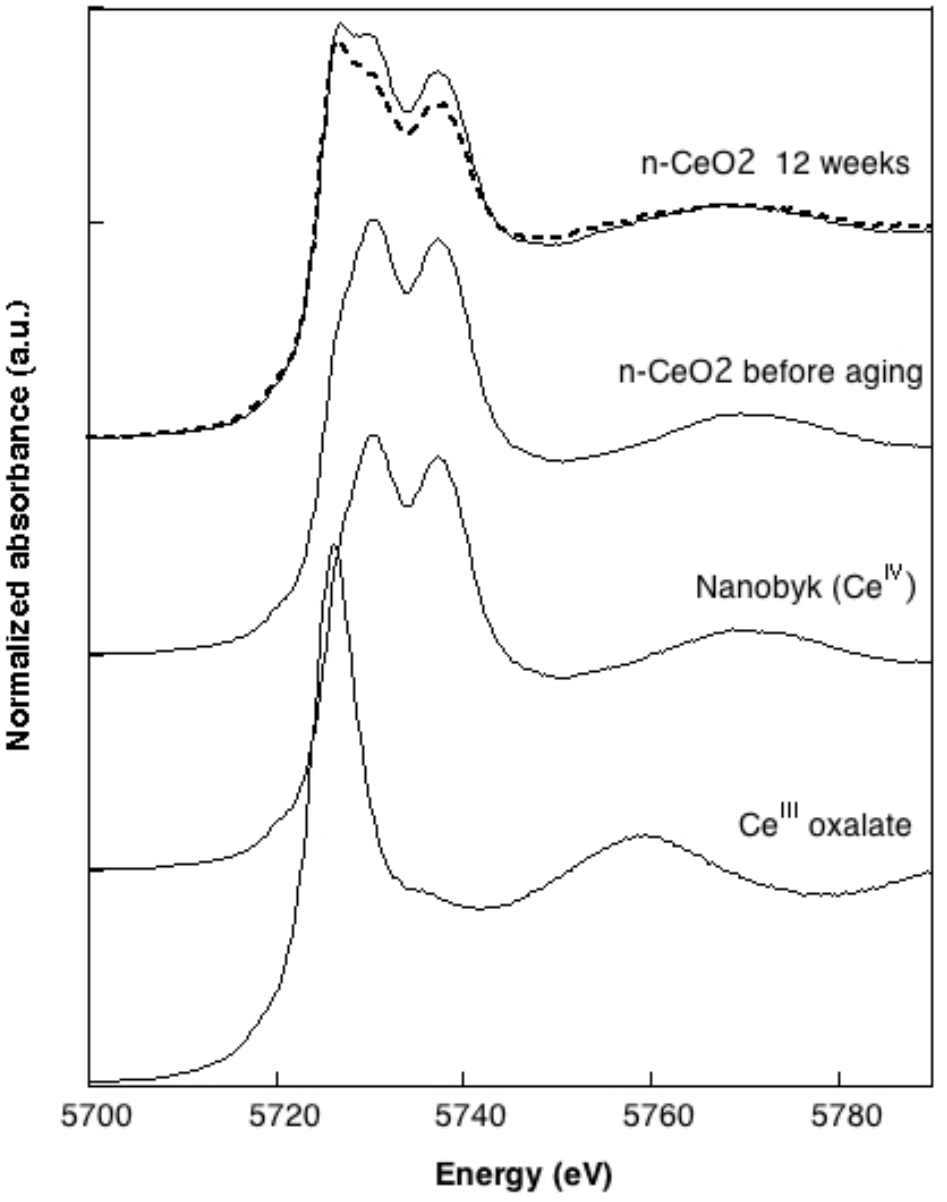
n-CeO2 12 weeks
n-CeO2 before aging
Nanobyk (Ce^{IV})
Ce^{III} oxalate
Normalized absorbance (a.u.)
5700
5720
5740
5760
5780
Energy (eV)

Supporting Information for:

Non-linear release dynamics for a CeO_2 nanomaterial embedded in a protective wood stain, due to matrix photo-degradation

Lorette Scifo [a,b], Perrine Chaurand [b], Nathan Bossa [b], Astrid Avellan [b], Mélanie Auffan [b], Armand Masion [b], Bernard Angeletti [b], Isabelle Kieffer [d], Jérôme Labille [b], Jean-Yves Bottero [b] and Jérôme Rose [b].

AFFILIATION.

[a] *Tecnalia-France, Montpellier, France.*

[b] *Aix Marseille Univ, CNRS, IRD, INRA, Coll France, CEREGE, Aix-en-Provence, France.*

[d] *OSUG-FAME, UMS 832 CNRS-Univ. Grenoble Alpes, F-38041, Grenoble, France*

CORRESPONDING AUTHOR FOOTNOTE:

Perrine Chaurand. E –mail : chaurand@cerege.fr

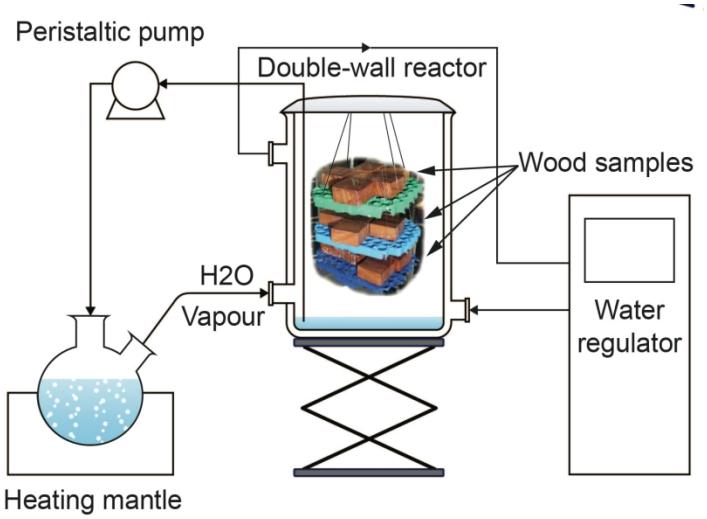

Figure S1. Homemade setup used for condensation phases in Suntest weathering (outside climate chamber). Ultrapure water is boiled in a flask. Vapor is directed towards a double-wall reactor where it is chilled and condenses at the surface of wood samples.

Sampling and physico-chemical characterization of "rain" waters in Suntest experiment.

40mL-aliquots of the water collected in beakers were taken after rain events #1 and #4 (Figure 1a) for further analyses. The beakers were then re-introduced in Suntest XLS+ with the remaining water volume. Whenever necessary, controlled amounts of Milli-Q water were added to the beakers to compensate for evaporation and prevent drying out. After spraying event #3 the whole water volume was collected and empty beakers were returned to the climate chamber for the longest 72h irradiation phase. pH and conductivity of all the aliquots were measured immediately after sampling. Redox potential was also measured once a week, on aliquots taken after rain event #3. Short sonication (15s) was applied before, but no stirring was maintained during the measurement of physico-chemical parameters.

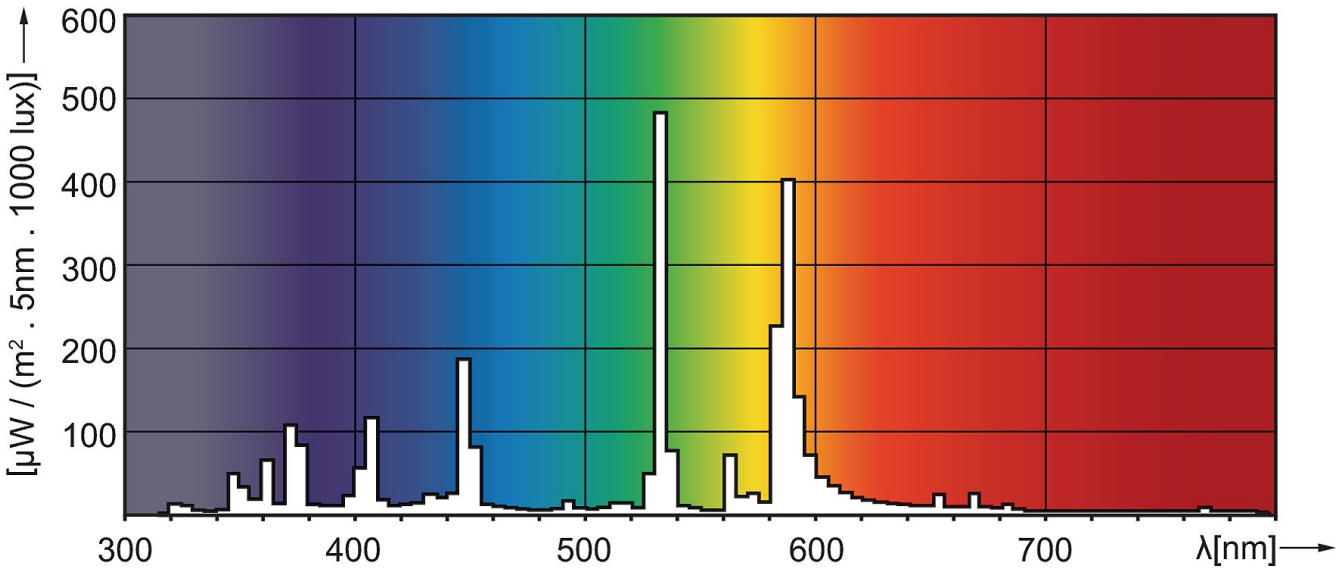

Figure S2. Emission spectra of Philips HPI-T Plus Metal Halide lamp. Downloaded from http://www.lighting.philips.fr/.

Table S3. Equivalence between weathering time in weeks, UV dose and radiant exposure in the 300nm - 800nm range for Suntest and batch experiments.

Weathering time (weeks)	Suntest experiment		Batch experiment	
	UV dose ($MJ.m^{-2}$)	Radiant exposure 300nm-800nm ($MJ.m^{-2}$)	UV dose ($MJ.m^{-2}$)	Radiant exposure 300nm-800nm ($MJ.m^{-2}$)
1	40	218	53	707
2	66	360	97	1367
3	111	607		
4	155	856		
5	199	1102		
6	245	1353		
7	290	1606		
8	335	1844		
9	379	2089		
10	424	2335		
11	469	2580		
12	513	2826		

Table S4. Defect density

Grade	Defect density
0	No defects, i.e undetected
1	Very little, i.e defects are rarely observed and are not significant
2	Few defects, i.e a small but significant amount of defects is observed
3	Moderate number of defects
4	Considerable number of defects
5	Dense concentration of defects

Table S5. Defect size

Grade	Defect size
0	Not visible at magnification x10
1	Only visible with optical magnification up to x10
2	Incipiently visible with normal or corrected vision
3	Clearly visible with normal or corrected vision (up to 0.5mm)
4	From 0.5mm to 5mm
5	Above 5 mm